

SENSOR AND SIMULATION NOTES

NOTE XLV

June 1967

ELECTROMAGNETIC SCATTERING FROM A CONDUCTING POST

by

R.W. Sassman,
R.W. Latham and A.G. Berger*

Northrop-Nortronics
Applied Research Department
Newbury Park, California

FOR PERIODICALS
PL/PA 10/27/94

ABSTRACT

In the design of layouts for electric and magnetic field measurements the electromagnetic scattering from nearby conducting objects must be taken into account and minimized to acceptable levels. Quantitative results of machine computations are presented here for the scattering of a vertically polarized time-harmonic plane wave by a perfectly conducting vertical post on a perfectly conducting horizontal plane. The upper half-space is taken to be either free space or a highly conducting simple medium. The incident wave is assumed to have wavelength (in free space) or skin depth (in the conducting medium) large compared with post radius, but not necessarily large compared with post height.

For the parallel polarization assumed, this problem is equivalent to that of an unloaded dipole far from ground, and in fact the program as written pertains to the dipole with arbitrary polarization of the incident wave.

Results are given in the form of normalized plots of scattered electric and magnetic field amplitudes as functions of distance from the post in the horizontal plane, and of radian wavelength or skin depth. Three ratios of post height to radius are treated: 10, 100, and 1000.

The mathematical formalism and machine codes are discussed, together with various checks, limiting forms, and physical interpretations of the results.

* Now at Douglas Aircraft Co., MSSD, Santa Monica, California.

ACKNOWLEDGEMENTS

This work was funded under Contract AF29(601)-6856. Guidance and encouragement were given generously by Capt. Carl Baum and Dr. John Darrah of AFWL. Dr. George Soules of Northrop-Nortronics made a number of valuable suggestions for improving the efficiency of the computer programs. Prof. Charles Papas of the California Institute of Technology has been our mentor, although we assign him no responsibility for the accuracy of the results.

CONTENTS

<u>SECTION</u>		<u>PAGE</u>
1.0	INTRODUCTION	6
2.0	ANALYSIS OF SCATTERED FIELDS	9
	2.1 FORMALISM	9
	2.2 COMPUTATIONAL TECHNIQUES	16
3.0	RESULTS	19
4.0	VERIFICATION AND COMMENTS ON THE RESULTS	58
	4.1 PREDICTED ACCURACY	58
	4.2 COMPARISON WITH THEORY	59
	4.3 COMPARISON WITH EXPERIMENT	62
5.0	COMPUTER PROGRAMS	64
	REFERENCES	66

LIST OF FIGURES

<u>Figure</u>		<u>Page</u>
1	Geometry of Post Scatterer	21
2	$\frac{\sigma}{\omega\epsilon} \ll 1$, $a/h = 0.1$, $E_{\theta}(\lambda/h)/E_0$ vs R/h	22
3	$H_{\phi}(\lambda/h)/H_0$ vs R/h	23
4	$E_{\theta}(R/h)/E_0$ vs λ/h	24
5	$H_{\phi}(R/h)/H_0$ vs λ/h	25
6	$H_{\phi}(\lambda/h)\cos\phi/H_0 = 0.1$ vs R/h	26
7	$H_{\phi}(\lambda/h)\cos\phi/H_0 = 0.01$ vs R/h ...	27
8	$a/h=0.01$, $E_{\theta}(\lambda/h)/E_0$ vs R/h	28
9	$H_{\phi}(\lambda/h)/H_0$ vs R/h	29
10	$E_{\theta}(R/h)/E_0$ vs λ/h	30
11	$H_{\phi}(R/h)/H_0$ vs λ/h	31
12	$H_{\phi}(\lambda/h)\cos\phi/H_0 = 0.1$ vs R/h	32
13	$H_{\phi}(\lambda/h)\cos\phi/H_0 = 0.01$ vs R/h ...	33
14	$a/h=0.001$, $E_{\theta}(\lambda/h)/E_0$ vs R/h	34
15	$H_{\phi}(\lambda/h)/H_0$ vs R/h	35
16	$E_{\theta}(R/h)/E_0$ vs λ/h	36
17	$H_{\phi}(R/h)/H_0$ vs λ/h	37
18	$H_{\phi}(\lambda/h)\cos\phi/H_0 = 0.1$ vs R/h	38
19	$H_{\phi}(\lambda/h)\cos\phi/H_0 = 0.01$ vs R/h ...	39
20	$\frac{\sigma}{\omega\epsilon} \gg 1$, $a/h=0.1$, $E_{\theta}(\lambda/h)/E_0$ vs R/h	40
21	$H_{\phi}(\lambda/h)/H_0$ vs R/h	41
22	$E_{\theta}(R/h)/E_0$ vs λ/h	42
23	$H_{\phi}(R/h)/H_0$ vs λ/h	43

24	$\frac{\sigma}{\omega\epsilon} \gg 1, a/h=0.1,$	$H_{\phi}(\kappa/h)\cos\phi/H_0 = 0.1$ vs R/h	44
25		$H_{\phi}(\kappa/h)\cos\phi/H_0 = 0.01$ vs R/h	45
26	$a/h=0.01,$	$E_{\theta}(\kappa/h)/E_0$ vs R/h	46
27		$H_{\phi}(\kappa/h)/H_0$ vs R/h	47
28		$E_{\theta}(R/h)/E_0$ vs κ/h	48
29		$H_{\phi}(R/h)/H_0$ vs κ/h	49
30		$H_{\phi}(\kappa/h)\cos\phi/H_0 = 0.1$ vs R/h	50
31		$H_{\phi}(\kappa/h)\cos\phi/H_0 = 0.01$ vs R/h	51
32	$a/h=0.001,$	$E_{\theta}(\kappa/h)/E_0$ vs R/h	52
33	$\frac{\sigma}{\omega\epsilon} \gg 1, a/h=0.001,$	$H_{\phi}(\kappa/h)/H_0$ vs R/h	53
34		$E_{\theta}(R/h)/E_0$ vs κ/h	54
35		$H_{\phi}(R/h)/H_0$ vs κ/h	55
36		$H_{\phi}(\kappa/h)\cos\phi/H_0 = 0.1$ vs R/h	56
37		$H_{\phi}(\kappa/h)\cos\phi/H_0 = 0.01$ vs R/h	57
38	A comparison with experiment for the first resonance of E_{θ}/E_0		63

SECTION 1.0
INTRODUCTION

Accurate "free-field" measurements of electromagnetic waves are notoriously difficult to make because scattering by conducting bodies in the vicinity of sensors always contribute to the total measured fields. Estimates of the magnitudes of scattered fields are made (at worst) by intuition or (at best) by semi-empirical methods. Anharmonicity of the incident waves and conductivity of the propagating medium often are additional complicating factors.

The results presented here are a first step toward obtaining quantitative estimates of such perturbing fields for a geometry of particular interest in measurements of the nuclear electromagnetic pulse. We shall treat the case in which the incident electromagnetic field is a harmonic plane wave having the time dependent function $e^{-i\omega t}$ and travelling parallel to an infinitely conducting plane. The perturbing scatterer is a solid, infinitely conducting post extending vertically from the plane. The incident wave is polarized with its electric vector parallel to the cylinder axis.

The problem is solved in two major steps. First, the currents induced on a set of zones on the post are computed in a self-consistent way. That is, the electromagnetic interactions of the zone currents are taken into account. Second, the scattered

field magnitudes are computed from the set of current elements, which for this purpose are assumed concentrated on the cylinder axis. Wavelengths are assumed large compared with post radius, but not necessarily large compared with post height. Results are presented here only for wavelengths ranging from very large values (the static limit) down through the first resonance, for which the scattered fields are greatest. Subject to the condition on post radius, higher resonances than the first may be accurately dealt with by increasing the number of zones and, consequently, computation time.

In order to investigate the effects of varying the propagation characteristics of the medium, computations were made for the case of both low-conductivity and of high-conductivity media above the infinitely conducting plane. That is, on the assumptions of conduction current very small or very large compared with displacement current.

Solution of this harmonic problem leads naturally to solution of transient problems which are closer to reality for EMP fields. In fact results obtained for the present free-space case can be used in conjunction with a Fourier inversion routine with relative ease, subject only to the availability of adequate machine storage and operating time. Bodies of more complex shape than the dipole can also be treated by the technique used here; the main limitation being that the number of current zones

required will be greater, and the matrix inversion will be more costly. The present version of this routine can invert matrices up to 1000 x 1000 in size, although no arrays larger than 512 x 512 were required for solution of the dipole scattering through the first resonance.

All this is relatively straightforward and physically realistic for a non-conducting propagation medium, and for a highly conducting or very distant ground plane. However, for realistic ionized media there are complications due to non-linear and dispersive effects. Also the ground plane in real situations is often neither highly nor very poorly conducting. These topics have been discussed in the literature as well as in earlier EMP notes, and undoubtedly will be subjects of further detailed treatments.

Note that rationalized MKSA units are used throughout.

SECTION 2.0

ANALYSIS OF SCATTERED FIELDS

The scattered fields due to a time-harmonic electromagnetic plane wave incident on a perfectly conducting solid post of finite length have been calculated. The incident wave is polarized with the electric field parallel to the axis of the post, which is assumed to rest on a perfectly conducting ground-plane. The cases in which the upper medium is non-conducting and in which it is linear and highly conducting are both treated.

The calculations have been made by numerically solving the rigorous integral equation for the total current on the post. This solution involves inverting a matrix, representing the kernel of the integral equation, by machine computation. The fields of interest were then calculated numerically using the integral representation of the electromagnetic fields due to a known current distribution.

Initial computations and shorter runs were performed on a CDC 3600 machine, and longer production runs on the CDC 6600 machine at Kirtland Air Force Base.

2.1 FORMALISM

The formulation of this problem is a specialization of that developed in a Northrop Report, NVR-2798, which presents a

general numerical method for solving problems of electromagnetic scattering from perfect conductors.¹ The approach used here is an application of the method to the special case of a cylindrical scatterer.

We begin the derivation of the general integral equation by recalling an integral representation for the magnetic field in a homogeneous medium.² We consider the case in which there may be sources outside our region of interest, and we call the field due to these sources H^{ex} . Thus:

$$\underline{H}(\underline{r}) = \underline{H}^{ex}(\underline{r}) + \nabla \times \int_{\text{all space}} G(\underline{r}, \underline{r}') \underline{J}(\underline{r}') dV', \quad (1)$$

where

$$G(\underline{r}, \underline{r}') = \frac{e^{ik|\underline{r}-\underline{r}'|}}{4\pi|\underline{r}-\underline{r}'|}, \quad \text{the free-space Green's function,}$$

$$\underline{J}(\underline{r}') = \text{the volume current density,}$$

$$k = \text{the propagation constant in the medium.}$$

This equation may be specialized for the case where there are only surface currents. Defining the surface current density $\underline{K}(\underline{r})$ and bringing the curl operator inside the integral, equation (1) may be rewritten in the form

$$\underline{H}(\underline{r}) = \underline{H}^{ex}(\underline{r}) + \int_{\text{surface}} \nabla G(\underline{r}, \underline{r}') \times \underline{K}(\underline{r}') d\sigma'. \quad (2)$$

Now let us take the cross product of this equation with the unit normal at some point \underline{r}_0 on the surface to which the currents are confined, obtaining

$$\underline{n}(\underline{r}_0) \times \underline{H}(\underline{r}) = \underline{n}(\underline{r}_0) \times \underline{H}^{\text{ex}}(\underline{r}) + \int_{\text{surface}} \underline{n}(\underline{r}_0) \times [\underline{G}(\underline{r}, \underline{r}') \times \underline{K}(\underline{r}')] d\sigma' \quad (3)$$

Now it may be shown¹ that when $\underline{r} \rightarrow \underline{r}_0$ equation (3) becomes

$$\underline{n}(\underline{r}_0) \times \underline{H}(\underline{r}_0) = \underline{n}(\underline{r}_0) \times \underline{H}^{\text{ex}}(\underline{r}_0) + \frac{1}{2} \underline{K}(\underline{r}_0) + \lim_{S_0 \rightarrow 0} \int_{S-S_0} \underline{n}(\underline{r}_0) \times [\underline{G}(\underline{r}_0, \underline{r}') \times \underline{K}(\underline{r}')] d\sigma', \quad (4)$$

where S_0 is a small element of surface surrounding \underline{r}_0 . The $\frac{1}{2} \underline{K}(\underline{r}_0)$ appears because of the singular nature of $\underline{G}(\underline{r}, \underline{r}')$. It may also be shown that the limit exists independent of the particular shape chosen for S_0 , so this is not really a "principal value" type integral, as it has sometimes mistakenly been called in the literature.

Now for a perfect conductor, by definition we have:

$$\underline{n} \times \underline{H} = \underline{K}.$$

Using this in equation (4) and making the simplifying notational change $\underline{r}_0 \rightarrow \underline{r}$, there results finally

$$\frac{1}{2} \underline{K}(\underline{r}) = \underline{K}^{\text{ex}}(\underline{r}) + \int \underline{n}(\underline{r}) \times [\underline{G}(\underline{r}, \underline{r}') \times \underline{K}(\underline{r}')] d\sigma', \quad (5)$$

where

$$\underline{K}^{\text{ex}}(\underline{r}) = \underline{n}(\underline{r}) \times \underline{H}^{\text{ex}}(\underline{r}),$$

and the integral is to be understood in the sense of equation (4). Now if a perfect conductor is immersed in a field due to some external sources which are known, then $\underline{K}^{\text{ex}}(\underline{r})$ may be calculated at each point on its surface. Equation (5) is then a vector surface integral equation for the determination of the total surface currents flowing on the body. Once this equation has been solved the total fields at any point in space may be calculated by again employing equation (2) or its equivalent form for the electric field²:

$$\underline{E}(\underline{r}) = \underline{E}^{\text{ex}}(\underline{r}) + i\omega\mu \int_{\text{surface}} \underline{\Gamma}(\underline{r}, \underline{r}') \cdot \underline{K}(\underline{r}') d\sigma', \quad (6)$$

where

$$\underline{\Gamma}(\underline{r}, \underline{r}') = \left\{ \underline{U} + \frac{1}{k^2} \nabla \nabla \right\} G(\underline{r}, \underline{r}') = \text{the free-space dyadic Green's function,}$$

$$\underline{U} = \text{the unit dyadic,}$$

$$\nabla \nabla = \text{the double gradient dyadic.}$$

The central problem, of course, is in solving equation (5). The general approach¹ involves imagining the surface as a large set of connected triangles, on each of which a constant current is assumed. However, this method will not be discussed in detail here as the cylinder is a rather special geometry for which certain simplifications are appropriate. For a plane wave incident on a cylindrical surface we can make the following substitutions:

$\underline{H}^{\text{ex}}(\underline{r}) = \underline{H}_0(\underline{r})e^{ik(\underline{p}\cdot\underline{r})} = \text{incident plane wave,}$

$\underline{n}(\underline{r}) = \underline{i} \cos\phi + \underline{j} \sin\phi = \text{unit normal on the cylindrical surface at azimuthal angle } \phi,$

$\underline{r} = a\underline{n}(\underline{r}) + z\underline{k} = \text{vector position on the cylindrical surface,}$

$\underline{i}, \underline{j}, \underline{k} = \text{rectangular-coordinate unit vectors (introduced for convenience),}$

$k = \text{propagation constant,}$

$\underline{p} = \text{unit vector in the direction of propagation of the incident wave.}$

The additional definitions of $\underline{n}(\underline{r})$ and \underline{r} on the top and bottom faces of the cylinder are obvious.

Then equation (5) becomes

$$\begin{aligned} \frac{1}{2} \underline{k}\cdot\underline{K}(\underline{r}) &= \underline{k}\cdot\underline{K}^{\text{ex}}(\underline{r}) + \lim_{S \rightarrow 0} \int_{S_1-S} \{ \underline{n}(\underline{r})\cdot\underline{K}(\underline{r}') (z-z') \\ &\quad - a[1-\underline{n}(\underline{r})\cdot\underline{n}(\underline{r}')][\underline{k}\cdot\underline{K}(\underline{r}')] \} f(R_1) d\sigma' \\ &\quad + \int_{S_2} \{ \underline{n}(\underline{r})\cdot\underline{K}(\underline{r}') (z\pm h) \} f(R_2) d\sigma', \end{aligned} \quad (7)$$

where S_1 is the side surface, S_2 and S_3 are the end surfaces, and

$$f(R) = \frac{(ikR-1)e^{ikR}}{4\pi R^3}.$$

Now we define, in terms of cylindrical coordinates (ρ, ϕ, z),

$$I_{S_1}(z) = \int_0^{2\pi} \underline{k} \cdot \underline{K}(r) a d\phi,$$

$$I_{S_2}(\rho) = \int_0^{2\pi} (\underline{i} \cos \phi + \underline{j} \sin \phi) \cdot \underline{K}(r) \rho d\phi,$$

$$I_{S_3}$$

and integrating equation (7) with the field point on the side of the cylinder we obtain

$$\begin{aligned} \frac{1}{2} I_{S_1}(z) &= I_{S_1}^{\text{ex}}(z) - \int_0^{\pi/2} \int_{-h}^h 8a^2 \sin^2 \psi f(R_1) I_{S_1}(z') dz' d\psi \\ &+ 2a(z+h) \int_0^{\pi} \int_0^a \cos \psi f(R_2) I_{S_2}(\rho') d\rho' d\psi \\ &+ 2a(z-h) \int_0^{\pi} \int_0^a \cos \psi f(R_3) I_{S_3}(\rho') d\rho' d\psi, \end{aligned}$$

with similar equations for the field point on the top or bottom surface.

Now from physical arguments and by inspection of the equations it becomes clear that

$$I_{S_2}(0) = I_{S_3}(0) = \left. \frac{dI_{S_2}(\rho)}{d\rho} \right|_{\rho=0} = \left. \frac{dI_{S_3}(\rho)}{d\rho} \right|_{\rho=0} = 0,$$

but

$$\left. \frac{d^2 I_{S_2}(\rho)}{d\rho^2} \right|_{\rho=0} \neq 0, \text{ and } \left. \frac{d^2 I_{S_3}(\rho)}{d\rho^2} \right|_{\rho=0} \neq 0.$$

Therefore assume:

$$I_{S_2}(\rho) = I_{S_2}(a) \frac{\rho^2}{a^2} = I_{S_1}(-h) \frac{\rho^2}{a^2},$$

$$I_{S_3}(\rho) = I_{S_3}(a) \frac{\rho^2}{a^2} = -I_{S_1}(h) \frac{\rho^2}{a^2}.$$

This assumption becomes better as $ka \rightarrow 0$, but is quite accurate even for $ka \approx 1$.

Then adopting the simplifying notation

$$I_{S_1}(z) \rightarrow I(z),$$

we have

$$\begin{aligned} \frac{1}{2} I(z) &= I^{\text{ex}}(z) - \int_0^{\pi/2} \int_{-h}^h 8a^2 \sin^2 \psi f(R_1) I(z') dz' d\psi \\ &+ \frac{2}{a} (z+h) I(-h) \int_0^{\pi} \int_0^a \cos \psi f(R_2) \rho^2 d\rho d\psi \\ &- \frac{2}{a} (z-h) I(h) \int_0^{\pi} \int_0^a \cos \psi f(R_3) \rho^2 d\rho d\psi, \end{aligned} \quad (8)$$

where

$$R_1^2 = (z-z')^2 + 4a^2 \sin^2 \psi,$$

$$R_2^2 = (z+h)^2 + z^2 + \rho^2 - 2a\rho \cos \psi,$$

$$R_3^2 = (z-h)^2 + a^2 + \rho^2 - 2a\rho \cos \psi,$$

$$I^{\text{ex}}(z) = i2\pi a e^{ikz \cos \theta} J_1(ka \sin \theta) H_x^{\text{ex}},$$

θ = angle of incidence with respect to the cylinder axis.

Equation 8 is the one which has been solved numerically.

2.2 COMPUTATIONAL TECHNIQUES

The numerical solution of equation (8) starts by replacing the integral by a finite sum of terms calculated on the assumption of constant currents on each of several small sections into which the interval $h \geq z \geq -h$ is divided.

Mathematically we define

$$\begin{aligned} U(x;a,b) &= 0 \text{ for } a > x > b, \\ &= 1 \text{ for } b > x > a. \end{aligned}$$

Then

$$I(a) = \sum_{j=0}^N I_j U(z; z_j, z_{j+1}). \quad (9)$$

Substituting this expression in equation (8) we may numerically compute the integral in terms of the I_j for any z . This computation is made for z -values corresponding to the centers of each of the zones implicit in equation (9). The right and left sides of equation (8) are then equated for each of these z -values, resulting in an equation of the form:

$$\frac{1}{2} I_i = I_i^{\text{ex}} + \sum_{j=0}^N A_{ij} I_j. \quad (10)$$

A certain amount of care must be taken in the numerical computation of the diagonal elements A_{ii} , because the corresponding integrand in equation (8) is singular for this

matrix element. However, the computations may be carried out with the help of a generalized elliptic integral, the details of which need not concern us here, as they are straightforward and tedious.

Equation (10) may now be written in terms of real and imaginary parts, and the corresponding large set of real algebraic equations for the I_j may be solved on a digital computer using a matrix inversion routine capable of handling a few hundred equations with sufficient accuracy. This routine has been developed as a mathematical tool and was used in the post calculations. Once the I_j variables have been determined they may be used in combination with equations (2), (6), and (9) to numerically compute the electromagnetic fields at any point in space.

The present case of a perfectly conducting cylindrical post mounted perpendicularly on a perfectly conducting plane is handled as outlined above for the symmetrical case of a plane wave incident normal to the axis of the post. The propagation constant used in the above formulation is then the propagation constant of the upper medium. Thus, for the incident plane wave³

$$\underline{H}^{ex} = \underline{H}_0 e^{i(k\underline{p} \cdot \underline{r} - \omega t)},$$

$$\underline{E}^{ex} = \underline{E}_0 e^{i(k\underline{p} \cdot \underline{r} - \omega t)},$$

$$\underline{p} \times \underline{E}^{ex} = (\omega \underline{H} / \kappa) \underline{H}^{ex}$$

$$\kappa^2 = \mu \epsilon \omega^2 + i \mu \sigma \omega.$$

For the "free-space" medium, with $\sigma/(\omega \epsilon) \ll 1$:

$$\kappa = \omega(\mu \epsilon)^{\frac{1}{2}},$$

$$\frac{E_0}{H_0} = (\mu/\epsilon)^{\frac{1}{2}} = Z_0 \approx 377 \text{ ohms.}$$

For the highly conducting medium, with $\sigma/(\omega \epsilon) \gg 1$:

$$\kappa = (1 + i)/\delta,$$

$$\delta = (\mu \sigma \omega / 2)^{-\frac{1}{2}} = \text{the skin depth,}$$

$$\frac{E_0}{H_0} = (\mu \omega \delta)^{\frac{1}{2}} (1 + i)^{-1}.$$

SECTION 3.0

RESULTS

Geometrical relationships are shown in Figure 1. It is to be noted that a post of height, h , on a highly conducting plane is equivalent to an isolated dipole of length $2h$ for these scattering computations. The scattered electric field is opposite in phase to the incident field, and thus cancels it at the post surface so as to meet the required boundary condition. The scattered magnetic field is azimuthal and parallel to the incident magnetic field on the side of the post which faces the source. Both fields are azimuthally uniform in the present approximation. In the case of the conducting medium there is an additional phase factor between the electric and magnetic vectors³, although it is not of special interest here.

In the following figures the results for the non-conducting medium are grouped before the results for the conducting media. In either case the scattered fields for post length-to-radius ratios of 10, 100, and 1000 are grouped. For each value of this ratio, normalized plots of scattered electric and magnetic fields are presented as functions of distance, with wavelength as a parameter; and as functions of wavelength, with distance as a parameter. Special "perturbing magnetic

field" plots are given. These are contours of scattered magnetic field components contributing 10% or 1% error to a measurement of the incident magnetic field. This component is largest for back or forward scattering, and there are nulls in the transverse plane. Obviously, no such nulls exist for the electric field.

The following symbols appear:

a/h = post radius/post height

$\frac{\sigma}{\omega\epsilon}$ = conductivity of the medium [mhos/meter] / 2π x frequency [hertz] x dielectric permittivity [farads/meter]),

E/E_0 = scattered electric-field amplitude/incident electric-field amplitude,

H/H_0 = scattered magnetic-field amplitude/incident magnetic-field amplitude,

R/h = distance from post axis to observation point on the plane/post height,

χ/h = wavelength/(2π x post height) = radian wavelength/h,

ϕ' = azimuthal angle, measured from the plane of incidence ($\phi' = \phi - \pi/2$).

δ/h = skin depth/post height.

NOTE: E_0 and H_0 for the case $\frac{\sigma}{\omega\epsilon} \gg 1$ are free-field values at the post axis. Thus no assumptions are made about attenuation of the incident wave.

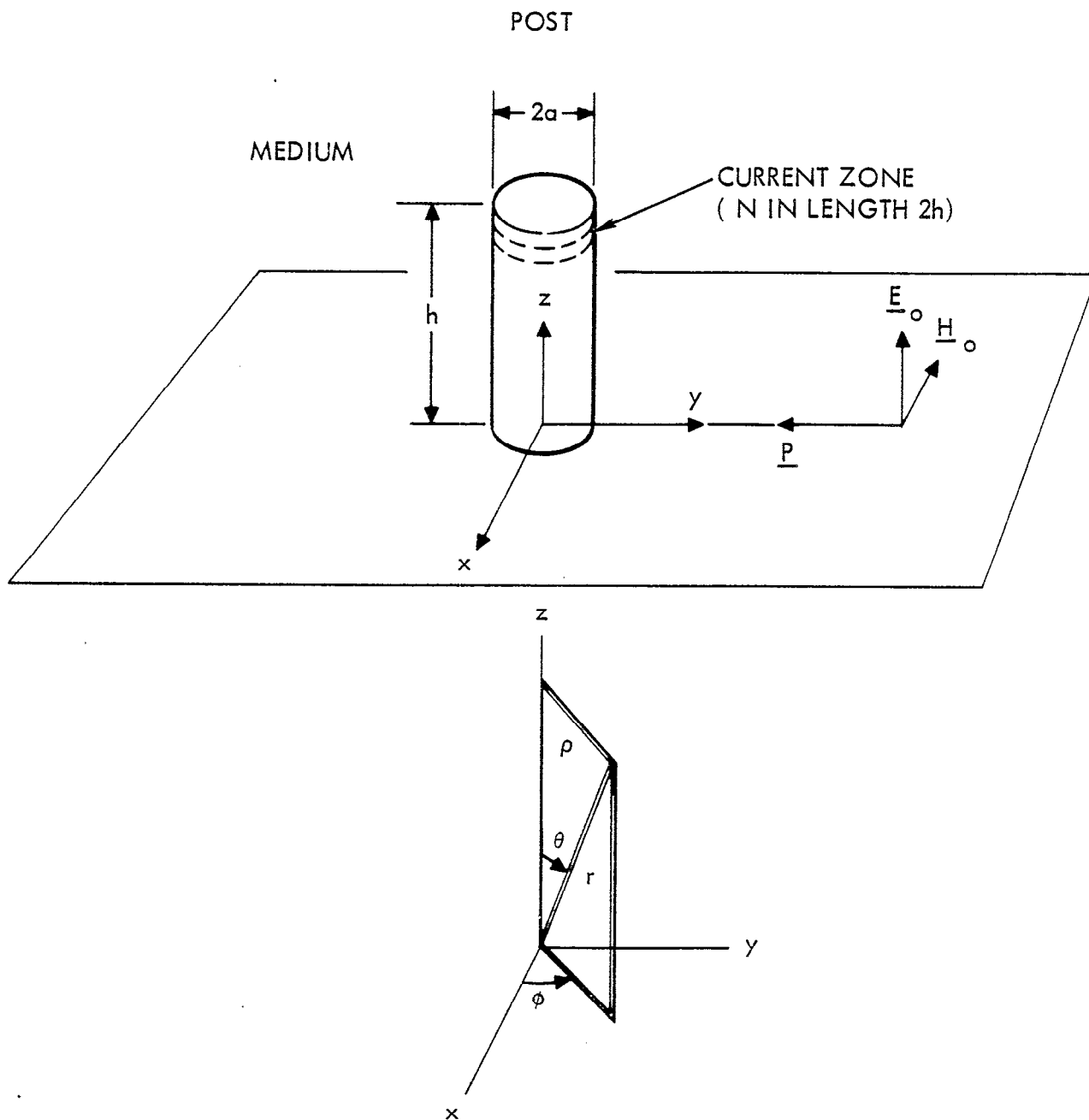


Figure 1. Geometry of Post Scatterer.

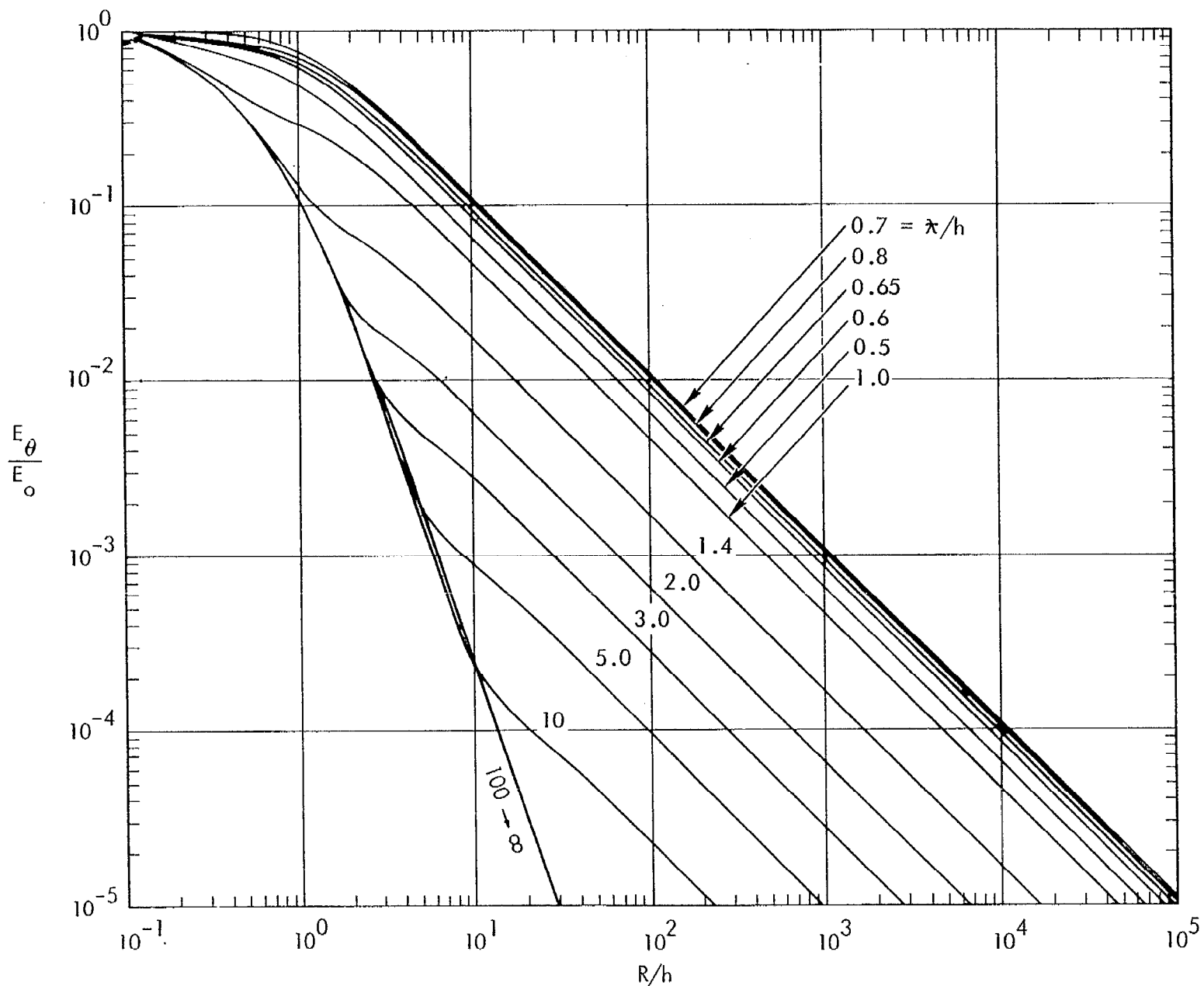


Figure 2. $\frac{J}{\omega \epsilon} \ll 1$, $a/h = 0.1$, $E_\theta(\kappa/h)/E_0$ vs R/h .

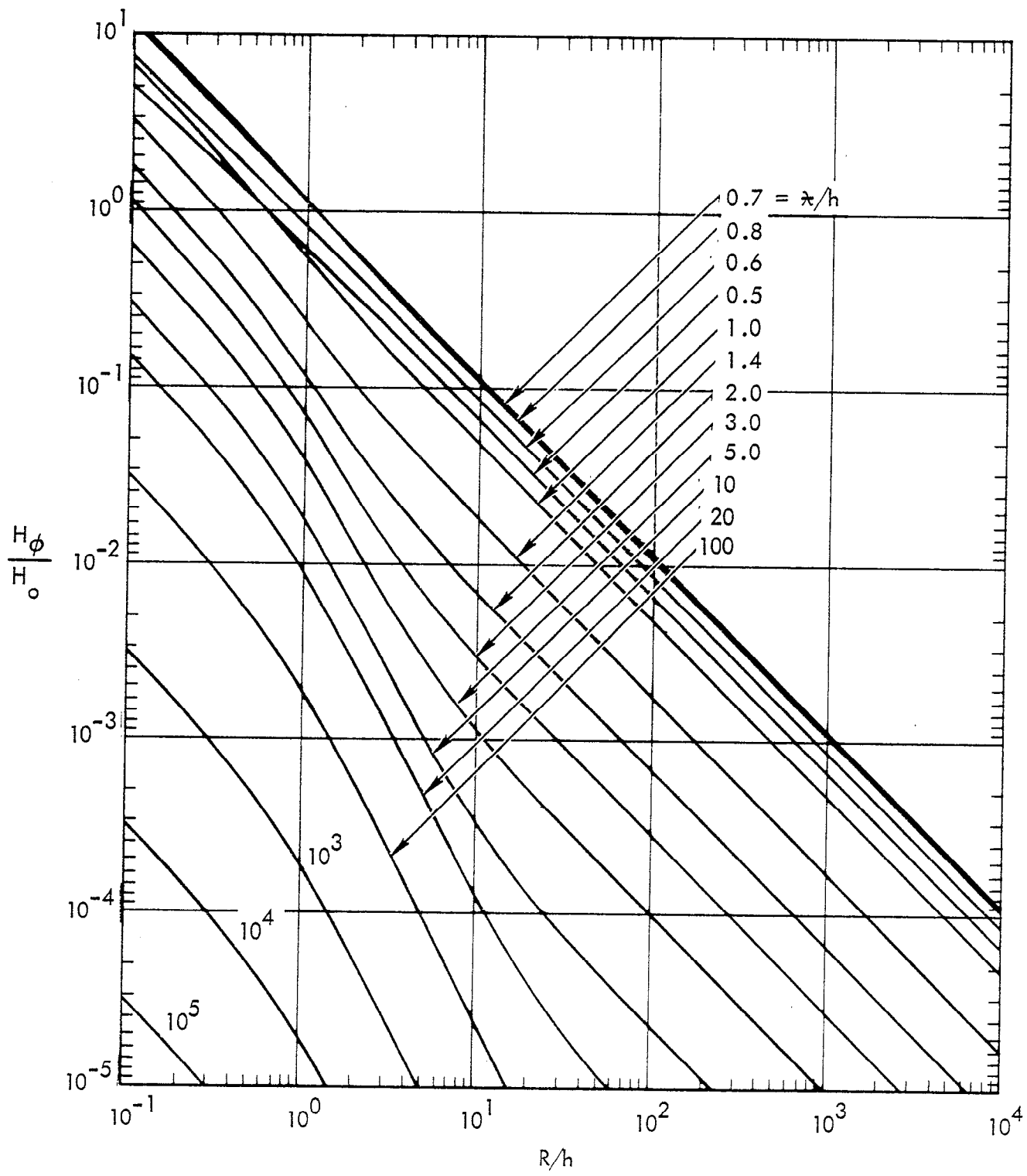


Figure 3. $\frac{\sigma}{\omega \epsilon} \ll 1$, $a/h = 0.1$, $H_0(\lambda/h)/H_0$ vs R/h .

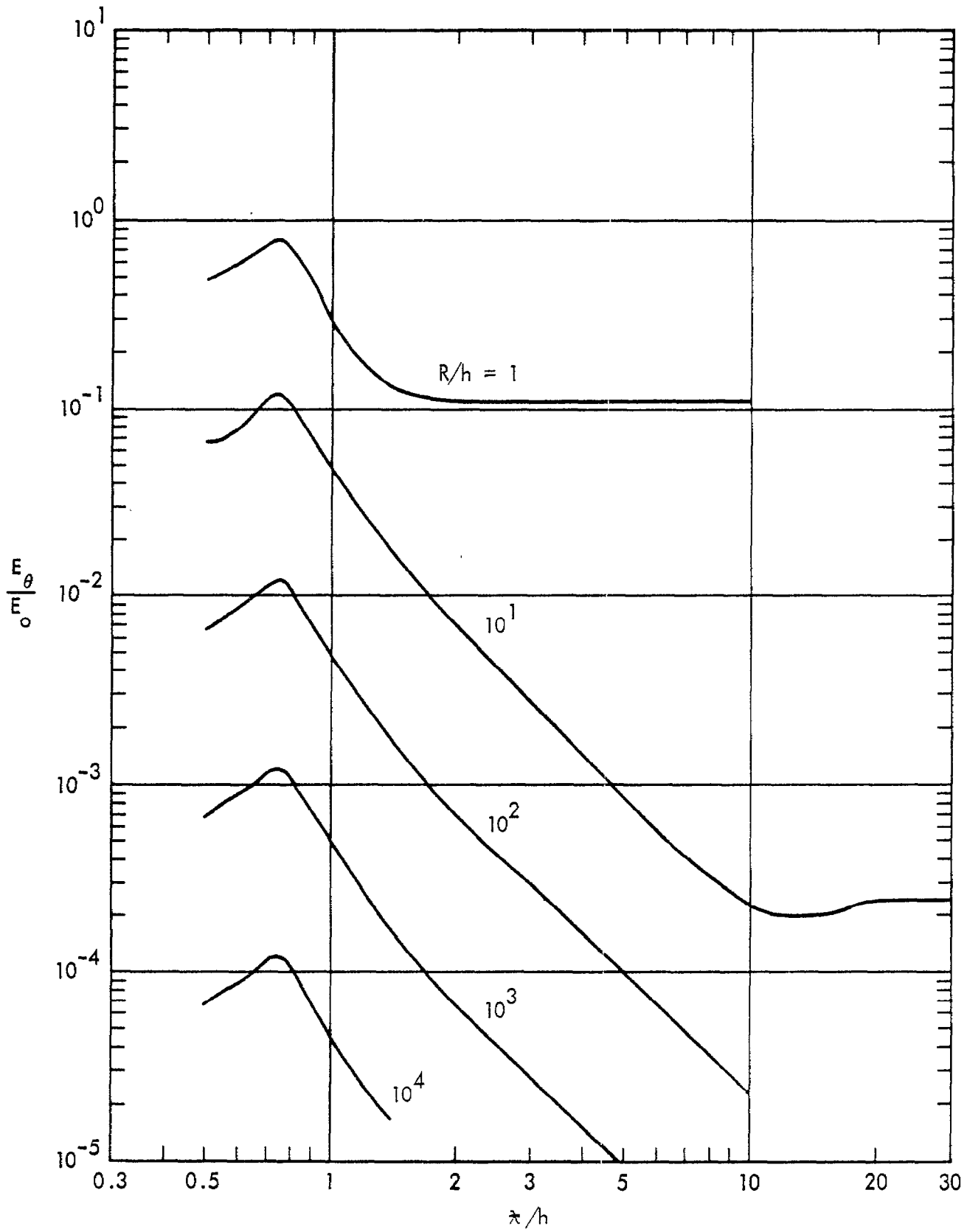


Figure 4. $\frac{\sigma}{\omega \epsilon} \ll 1$, $a/h = 0.1$, $E_0(R/h)/E_0$ vs k/h .

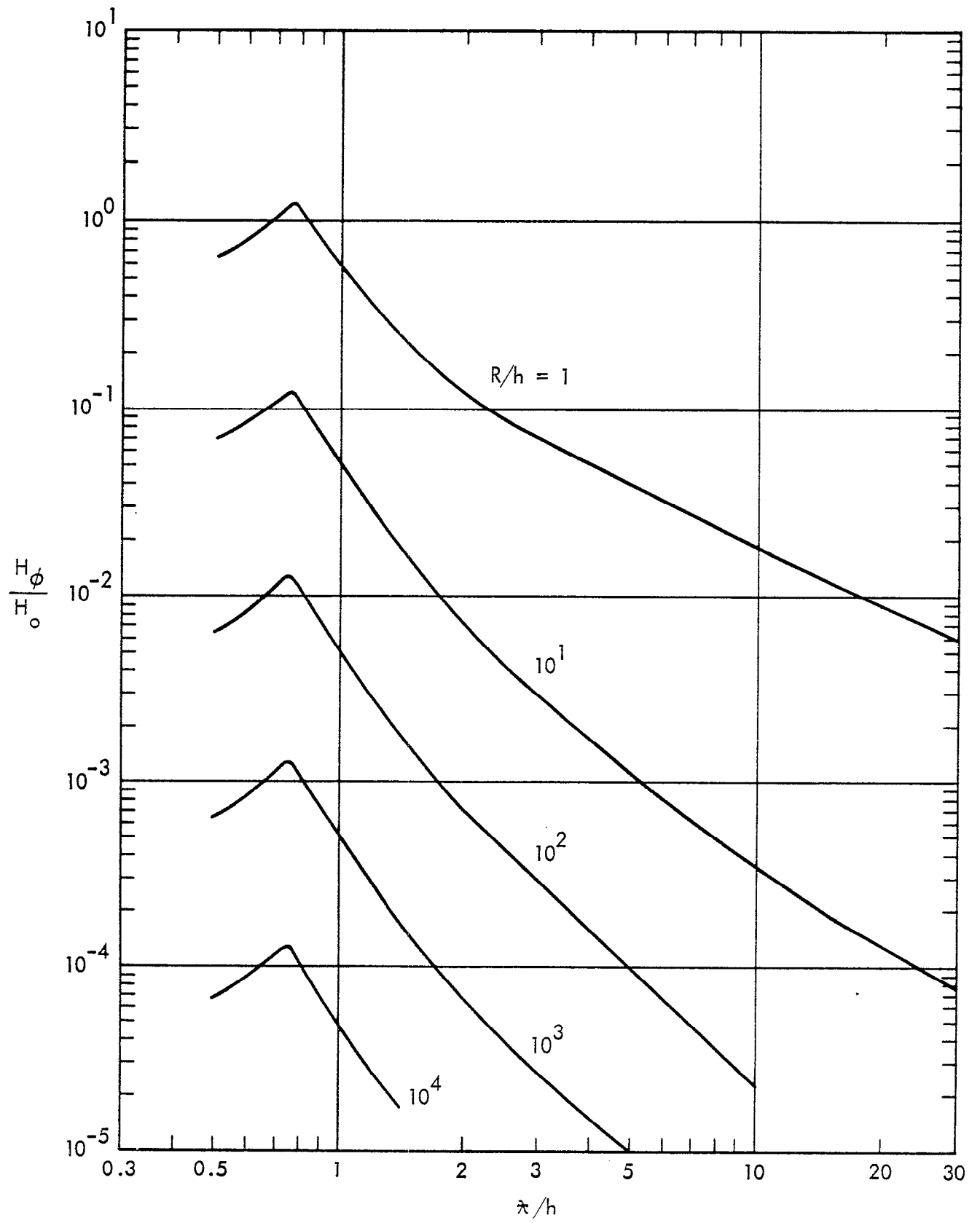


Figure 5. $\frac{\sigma}{\omega \epsilon} \ll 1$, $a/h = 0.1$, $H_0(R/h)/H_0$ vs κ/h .

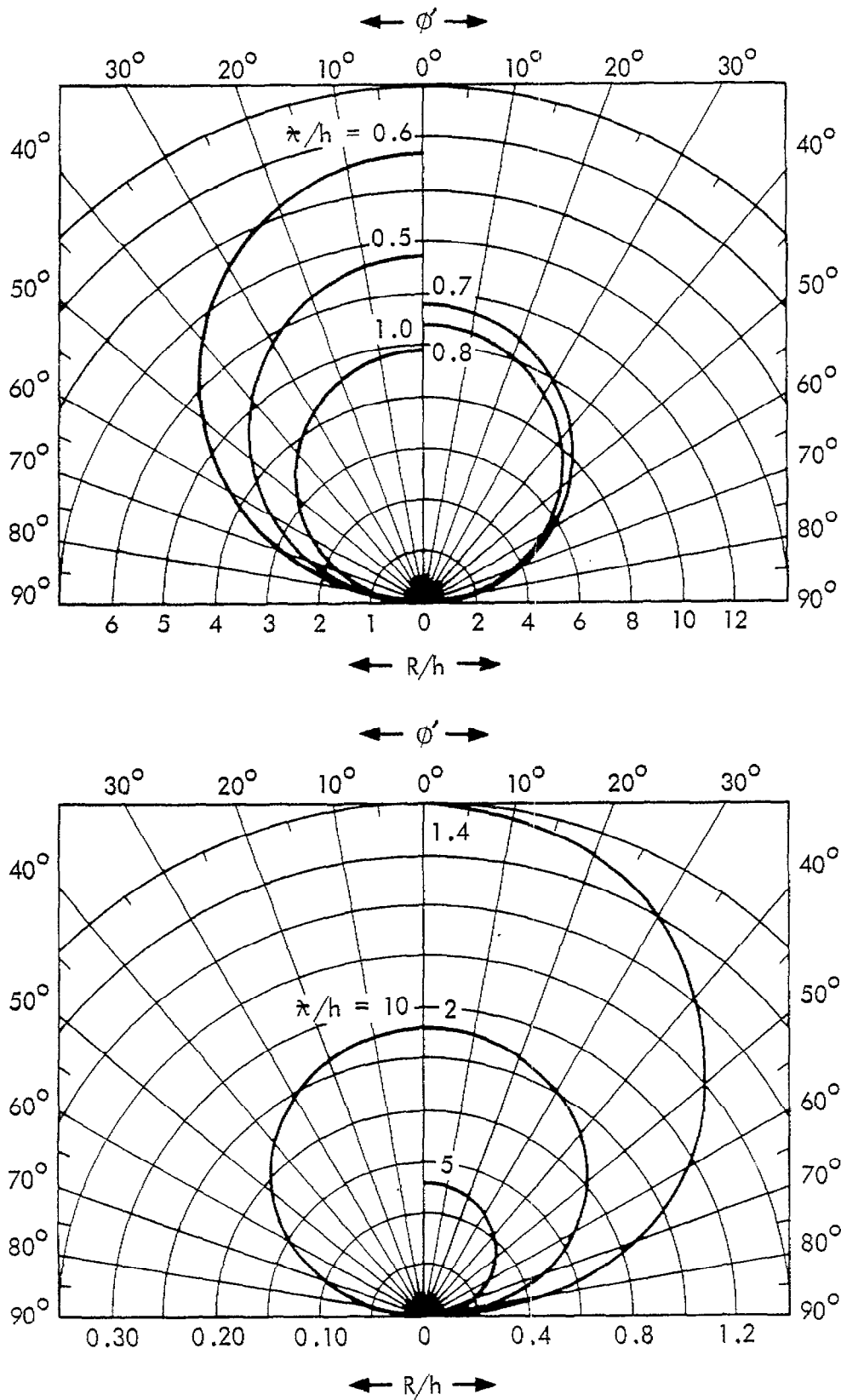


Figure 6. $\frac{\sigma}{\omega c} \ll 1$, $a/h = 0.1$, $H_\phi(\kappa/h)\cos\phi/H_0 = 0.1$ vs R/h .

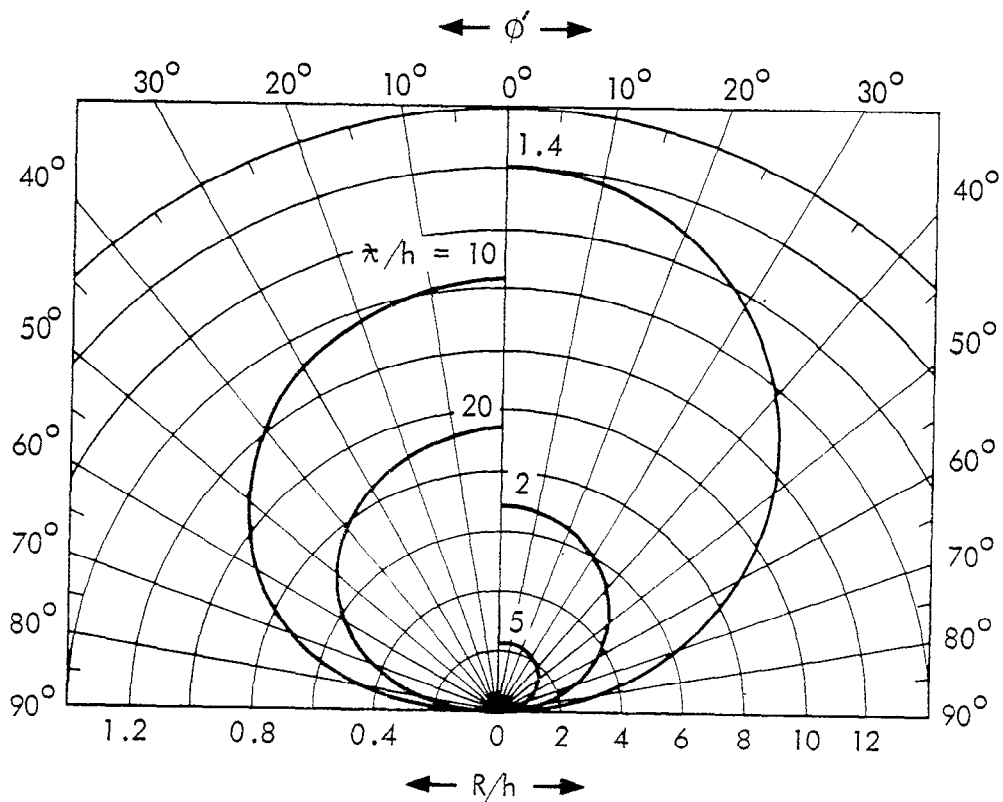
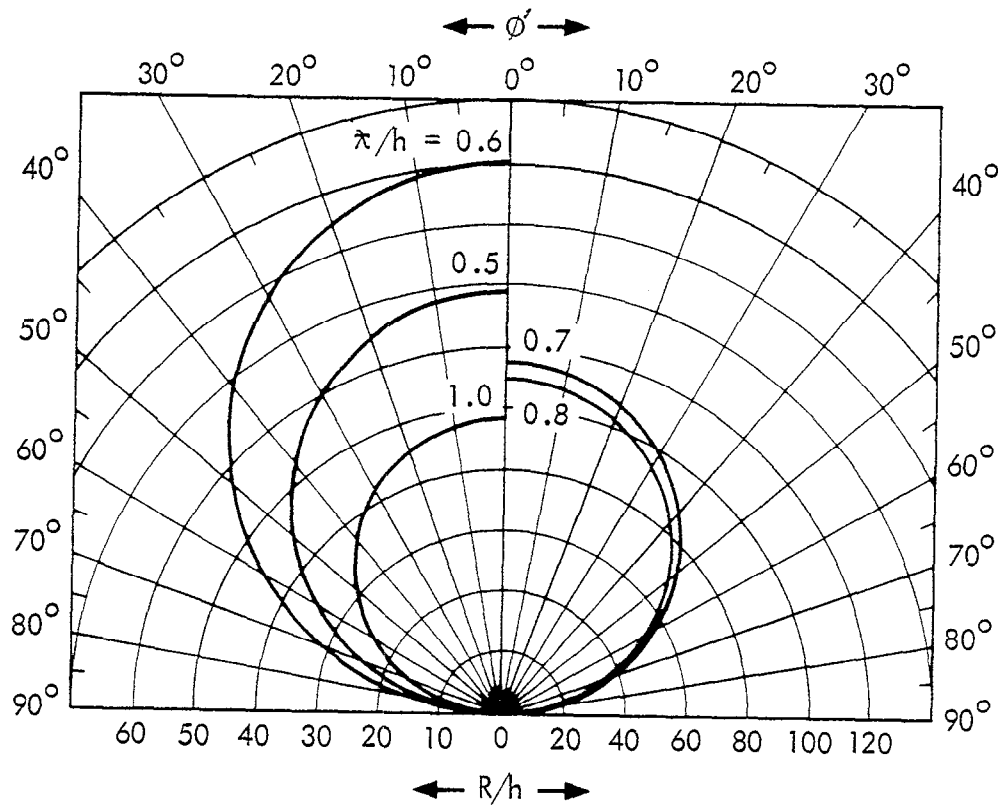


Figure 7. $\frac{\sigma}{\omega \epsilon} \ll 1$, $a/h = 0.1$, $H_\phi(\lambda/h) \cos \phi' / H_0 = 0.01$ vs R/h .

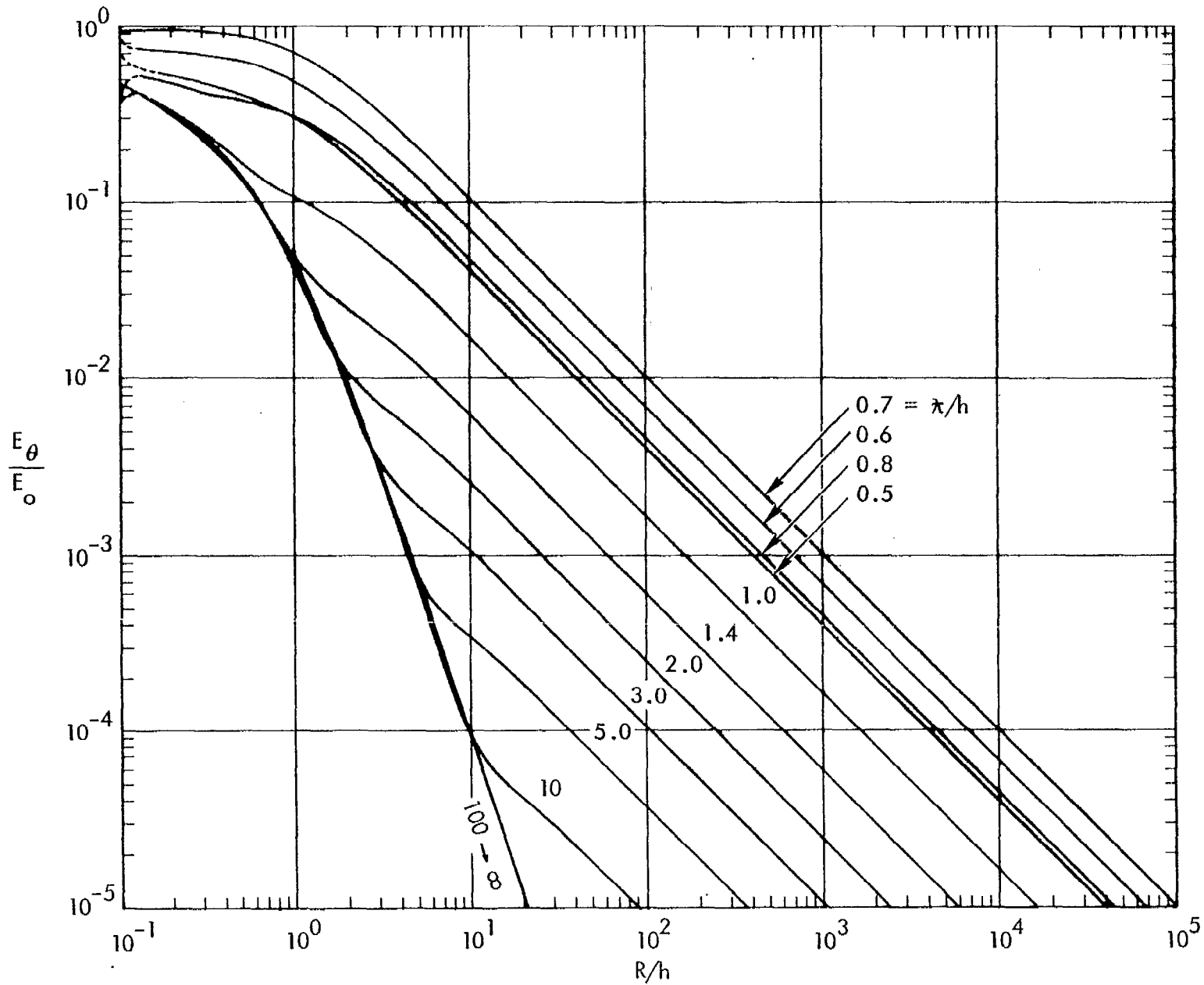


Figure 8. $\frac{\sigma}{\omega \epsilon} \ll 1$, $a/h = 0.01$, $E_\theta(\kappa/h)/E_0$ vs R/h .

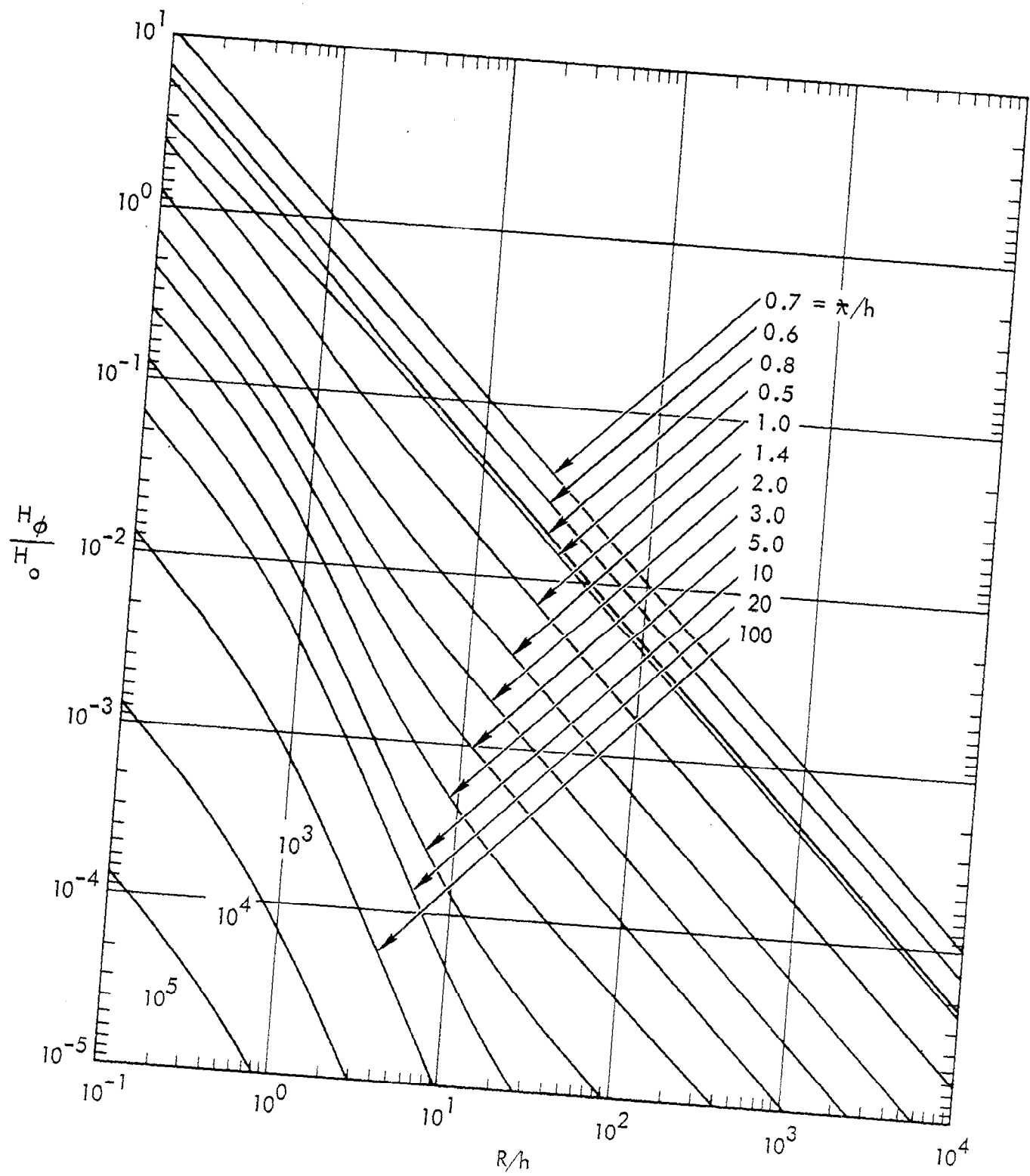


Figure 2. $\frac{\sigma}{\omega c} \ll 1$, $a/h = 0.01$, $H_0(\kappa/h)/H_0$ vs R/h .

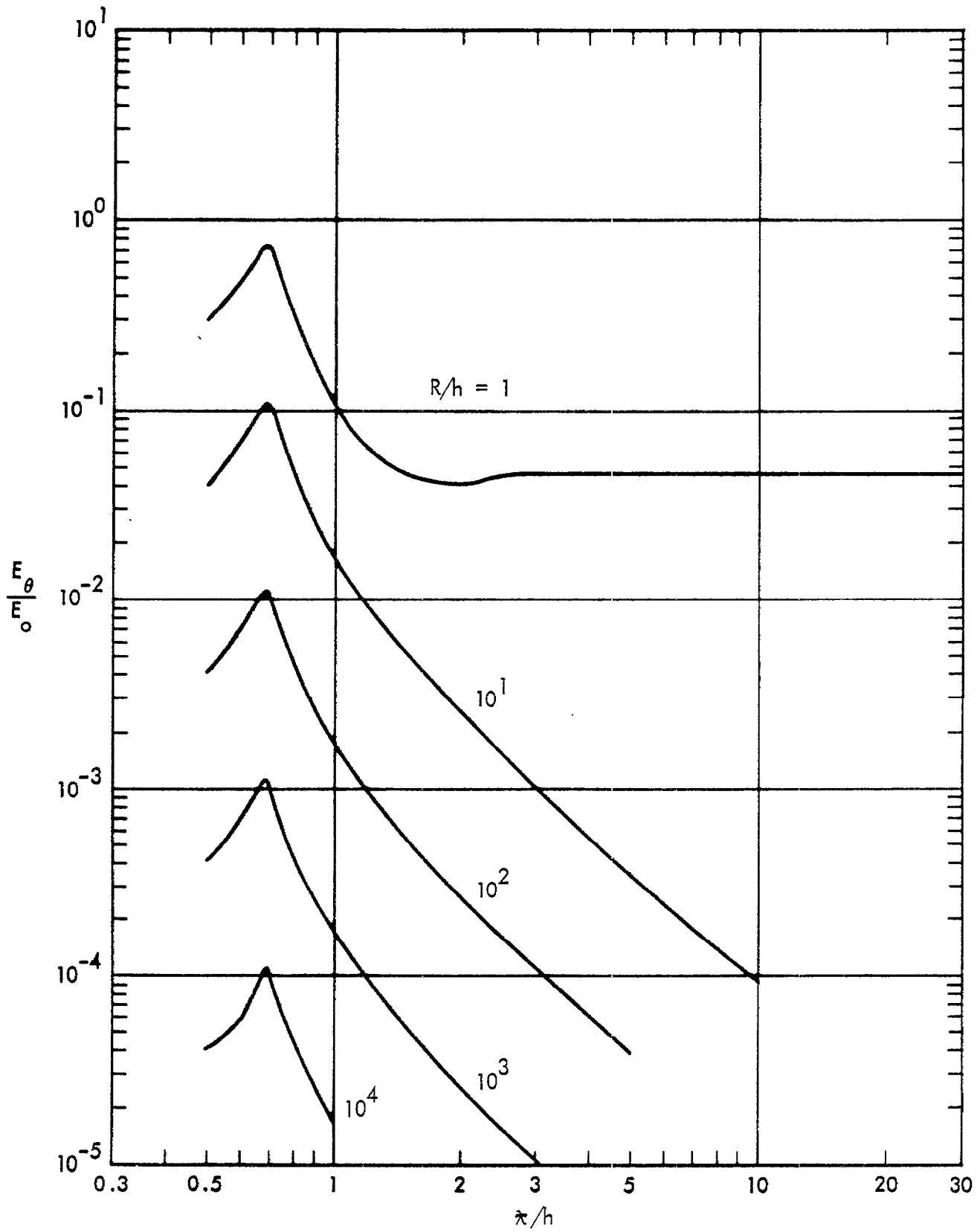


Figure 10. $\frac{\sigma}{\omega\epsilon} \ll 1$, $a/h = 0.01$, $E_{\theta}(R/h)/E_0$ vs κ/h .

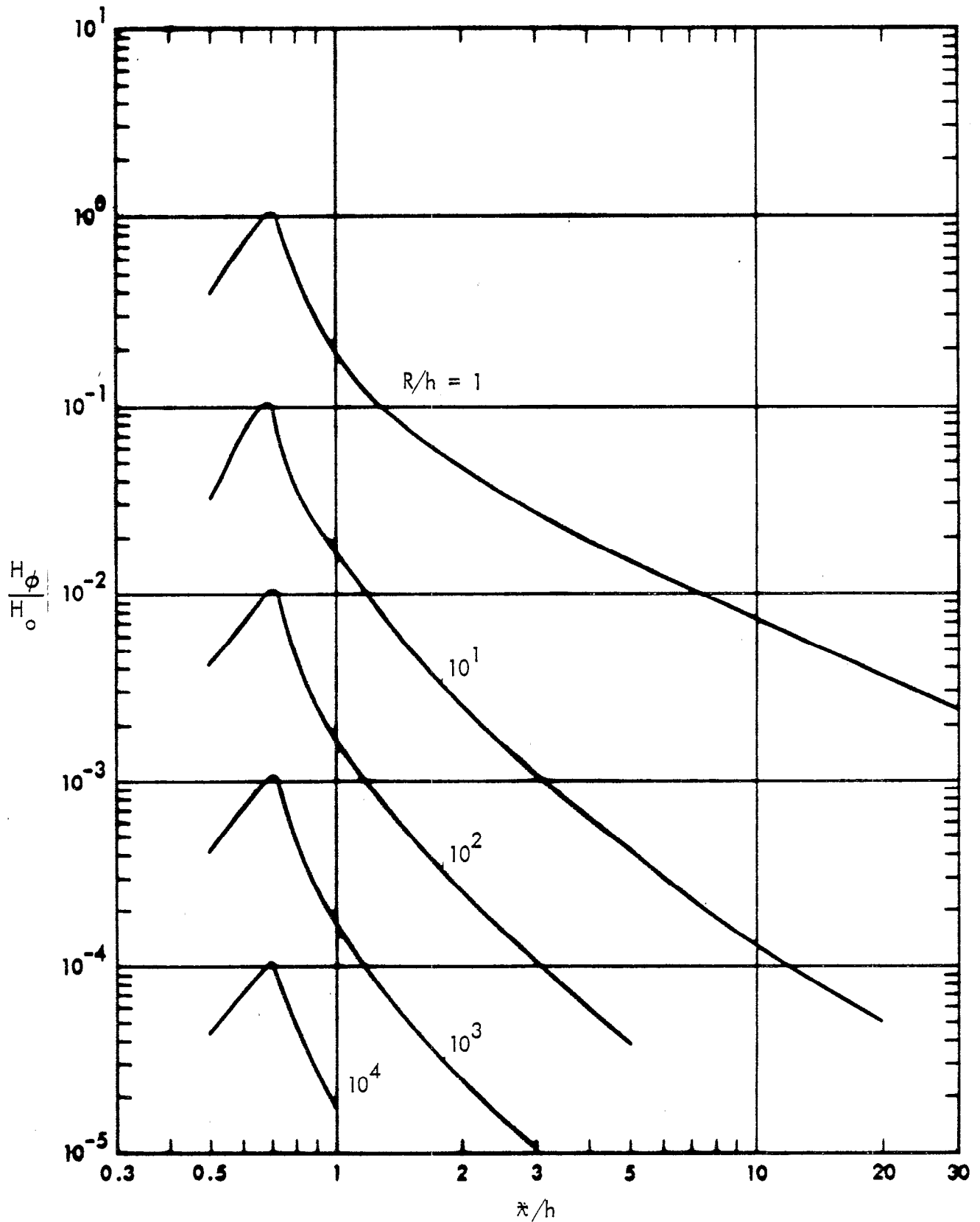


Figure 11. $\frac{\sigma}{\omega \epsilon} \ll 1$, $a/h = 0.01$, $H_\phi(R/h)/H_0$ vs κ/h .

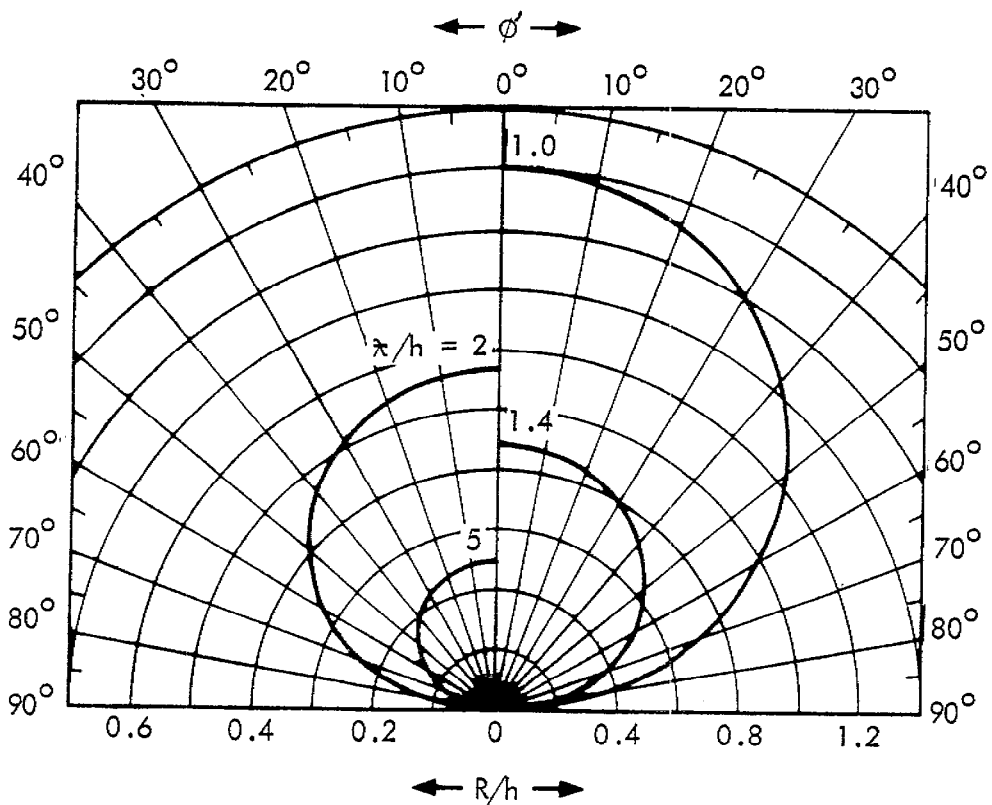
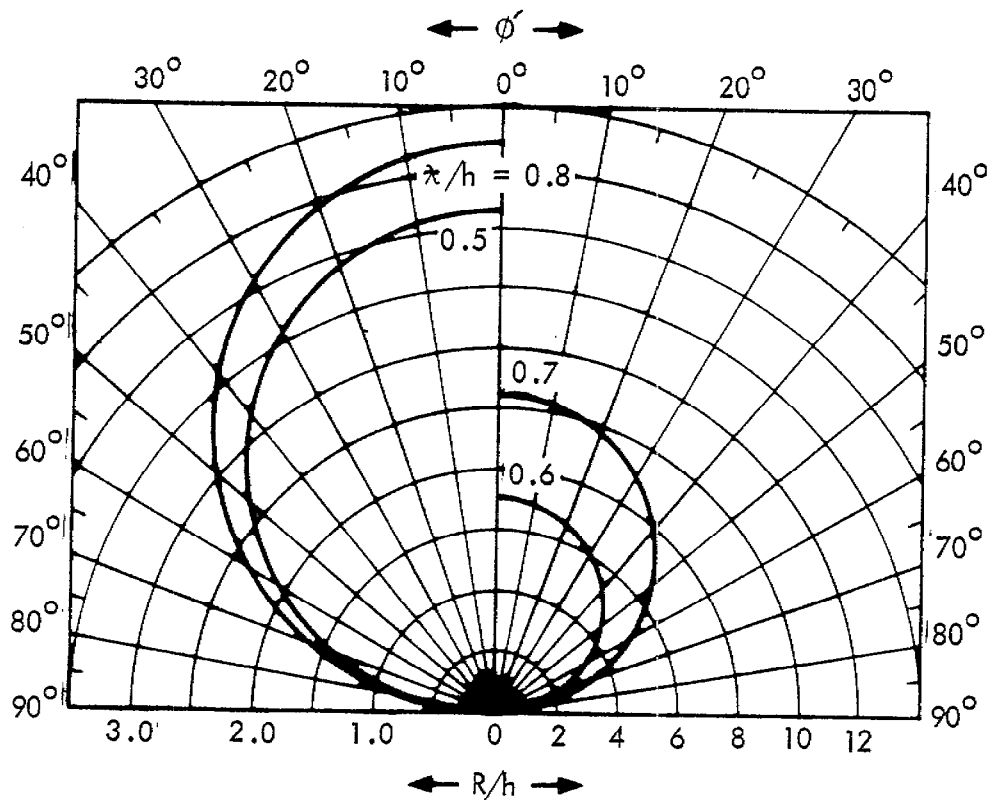


Figure 12. $\frac{\sigma}{w\epsilon} \ll 1$, $a/h = 0.01$, $H_\phi(\lambda/h)\cos\phi/H_0 = 0.1$ vs R/h .

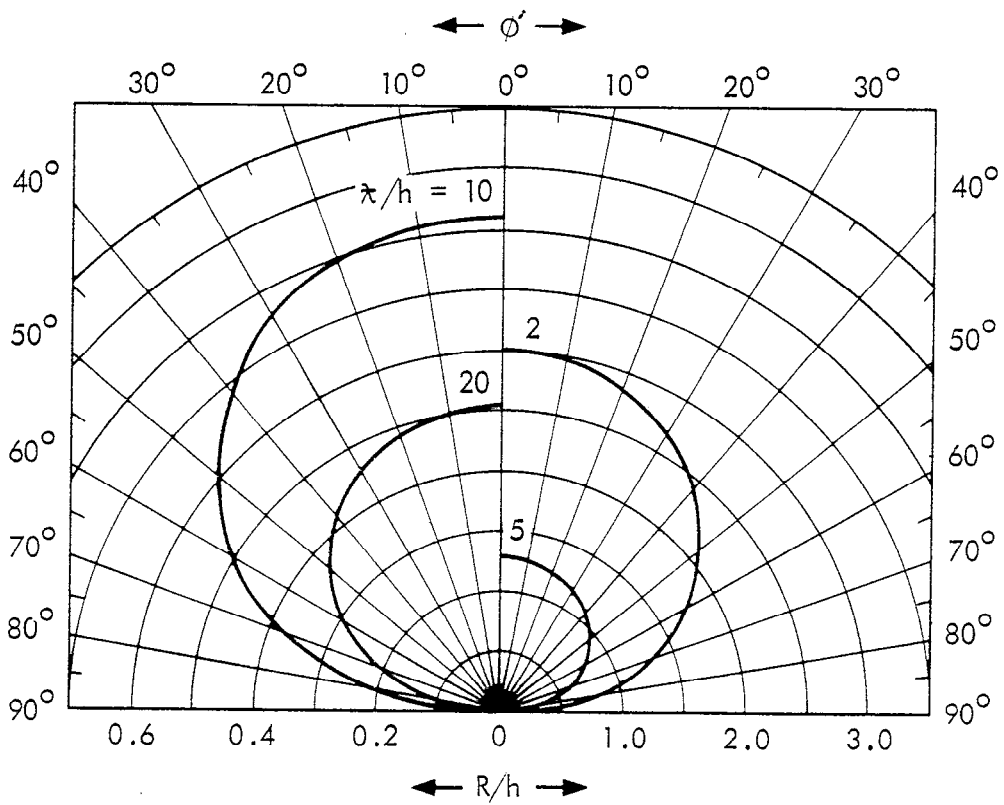
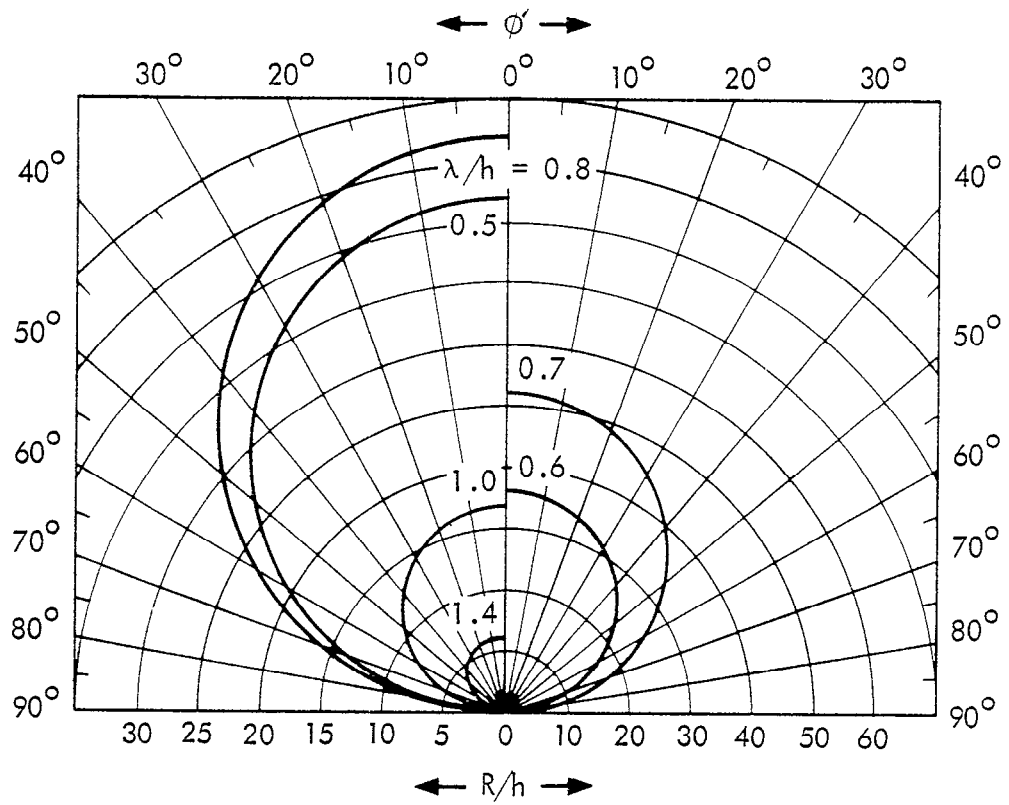
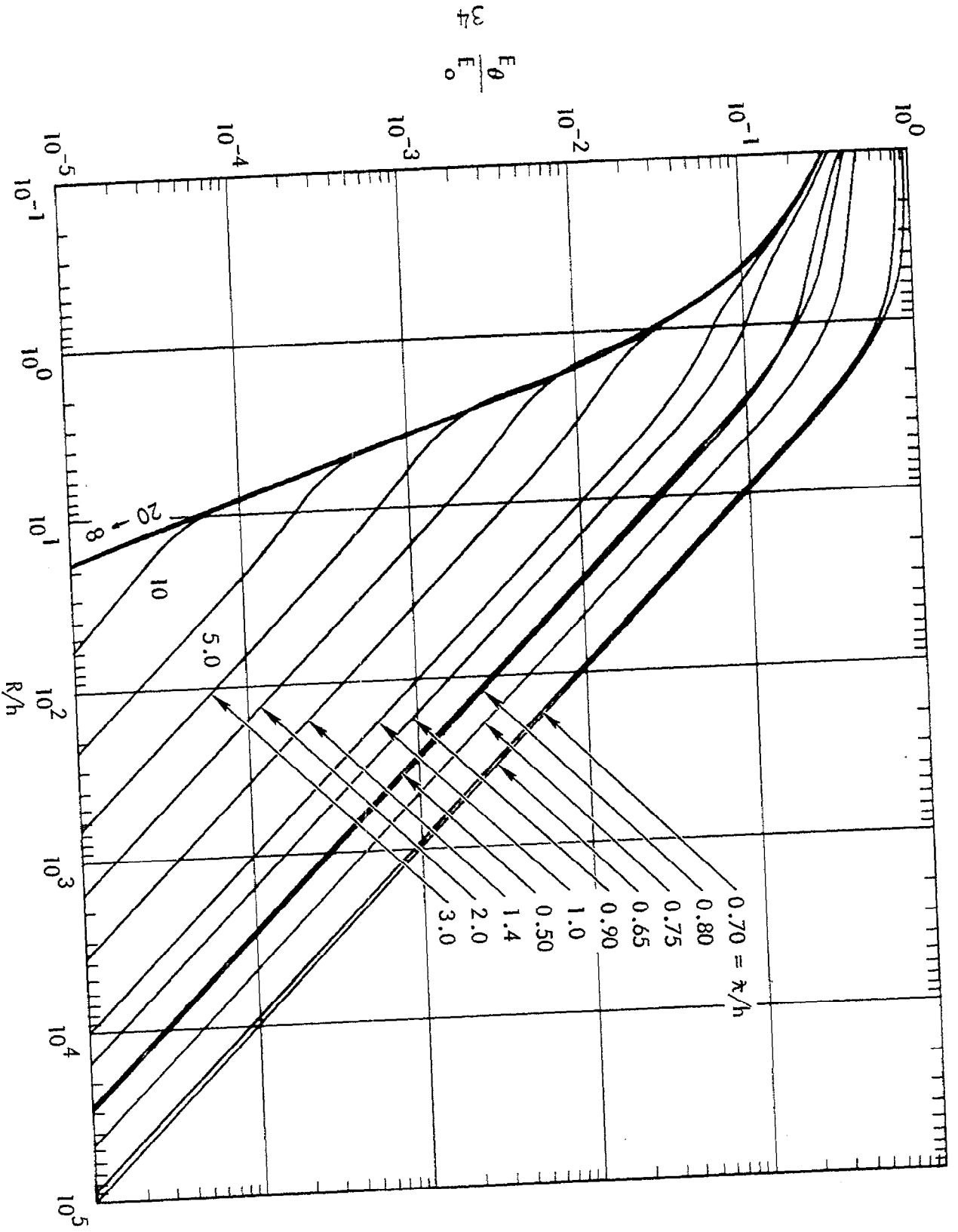


Figure 13. $\frac{\sigma}{\omega \epsilon} \ll 1$, $a/h = 0.01$, $H_\phi(\kappa/h) \cos \phi' / H_0 = 0.01$ vs R/h .



34
 $\frac{E_\theta}{E_0}$

Figure 14. $\frac{\sigma}{we} \ll 1, a/h = 0.001, E_\theta(\kappa/h)/E_c$ vs R/h .

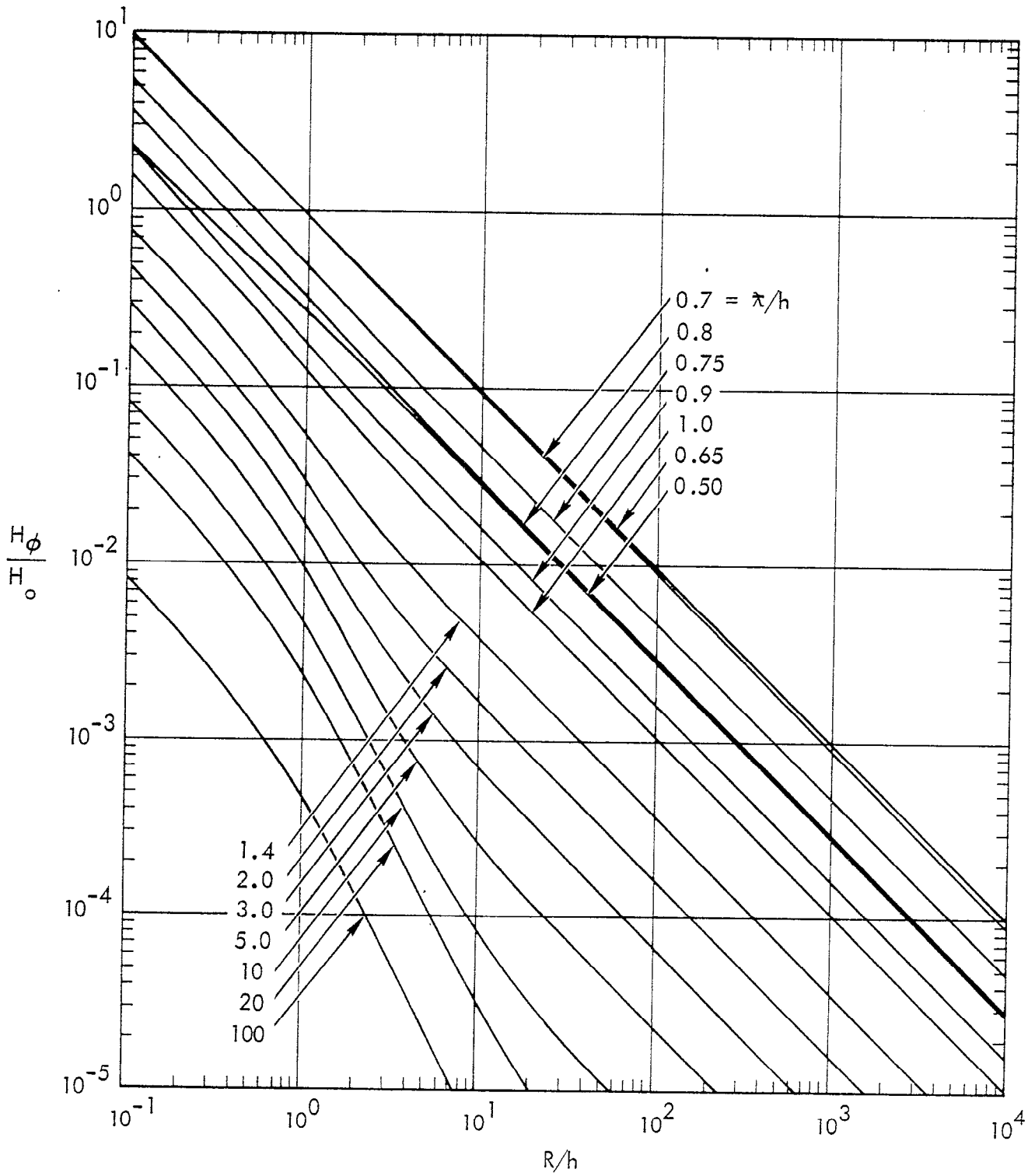


Figure 15. $\frac{\sigma}{\omega \epsilon} \ll 1$, $a/h = 0.001$, $H_\phi(\lambda/h)/H_0$ vs R/h

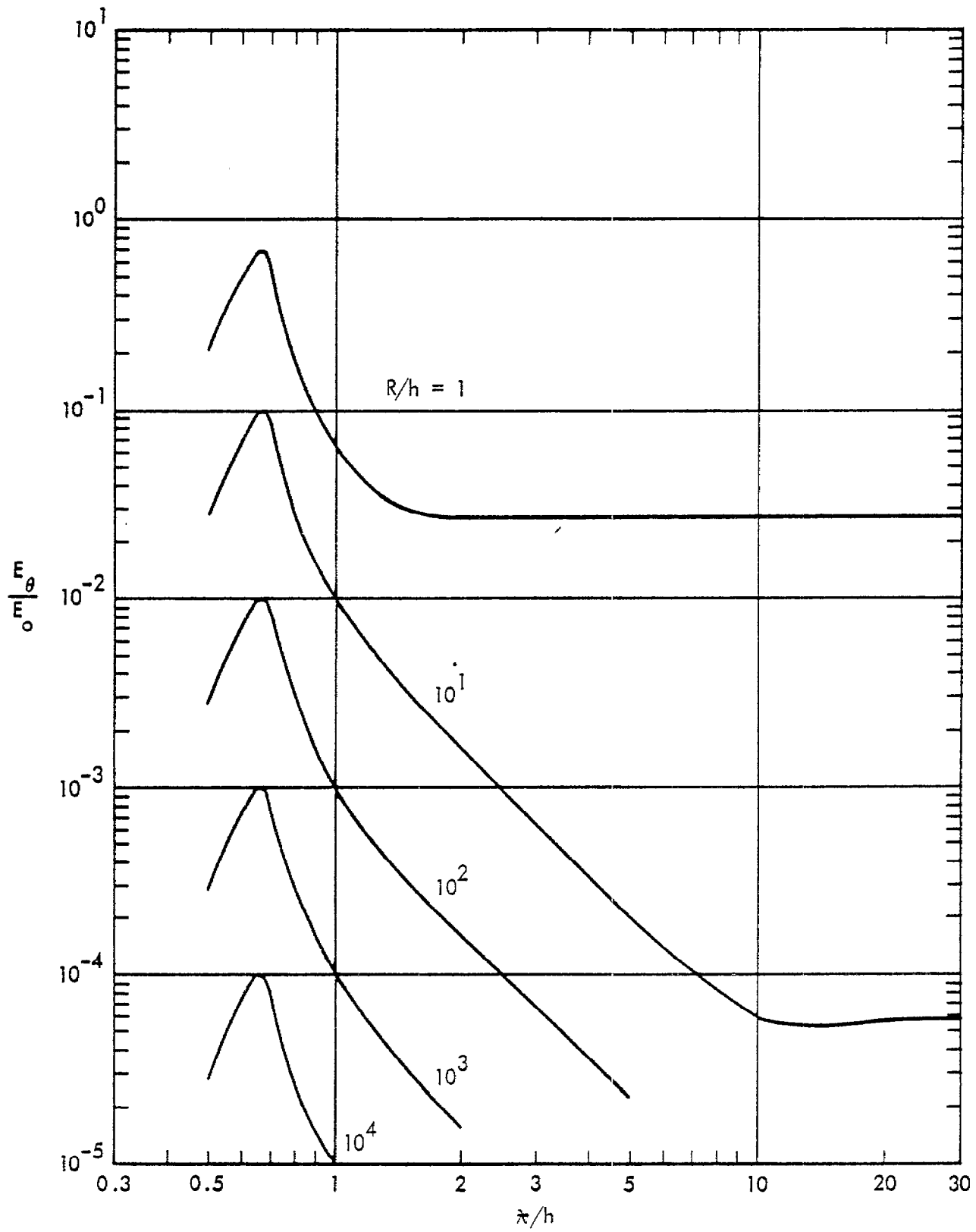


Figure 16. $\frac{\sigma}{\omega^2} \ll 1$, $a/h = 0.1$, $E_0(R/h)/E_0$ vs λ/h

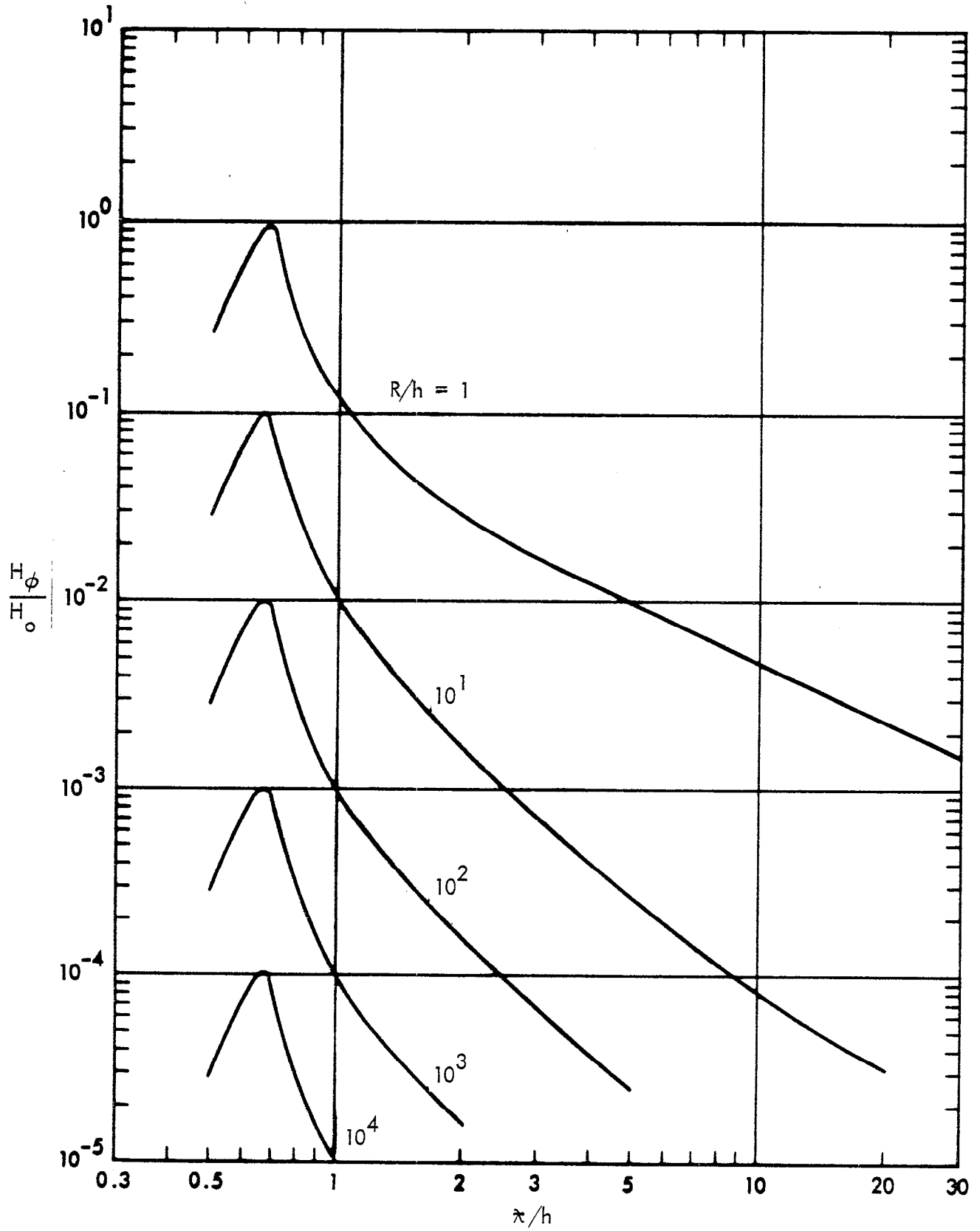


Figure 17. $\frac{\sigma}{\omega \epsilon} \ll 1$, $a/h = 0.001$, $H_0(R/h)/H_\phi$ vs λ/h .

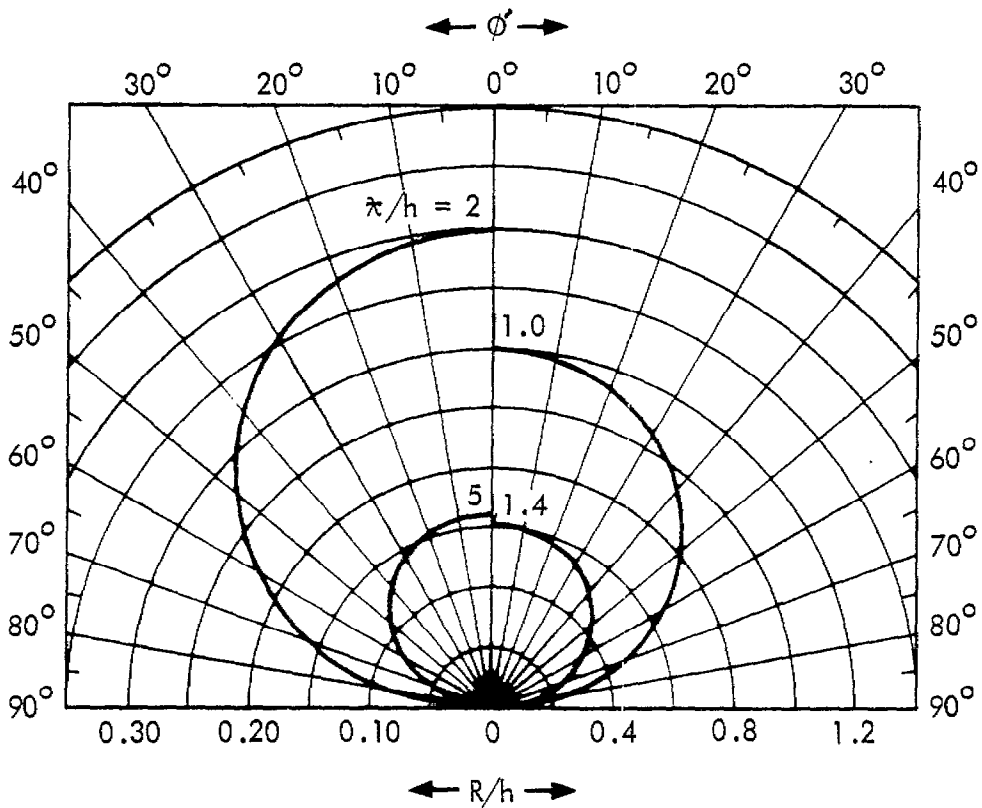
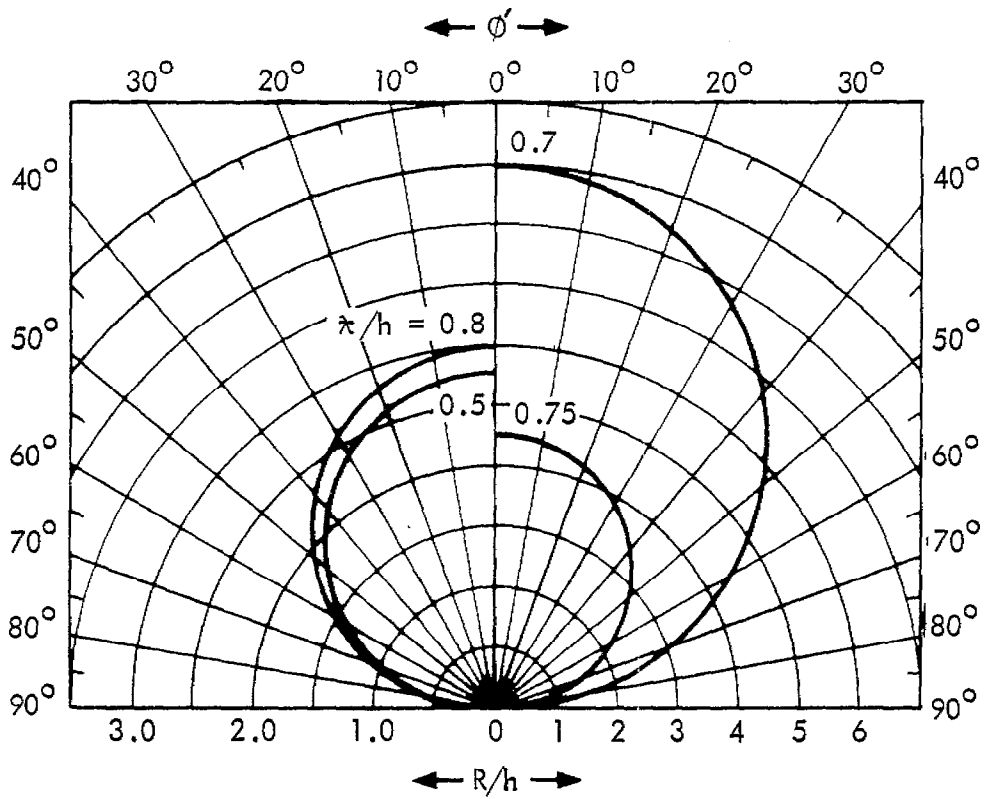


Figure 18. $\frac{\sigma}{\omega\epsilon} \ll 1$, $a/h = 0.001$, $H_\phi(\lambda/h)\cos\phi/H_0 = 0.1$ vs R/h .

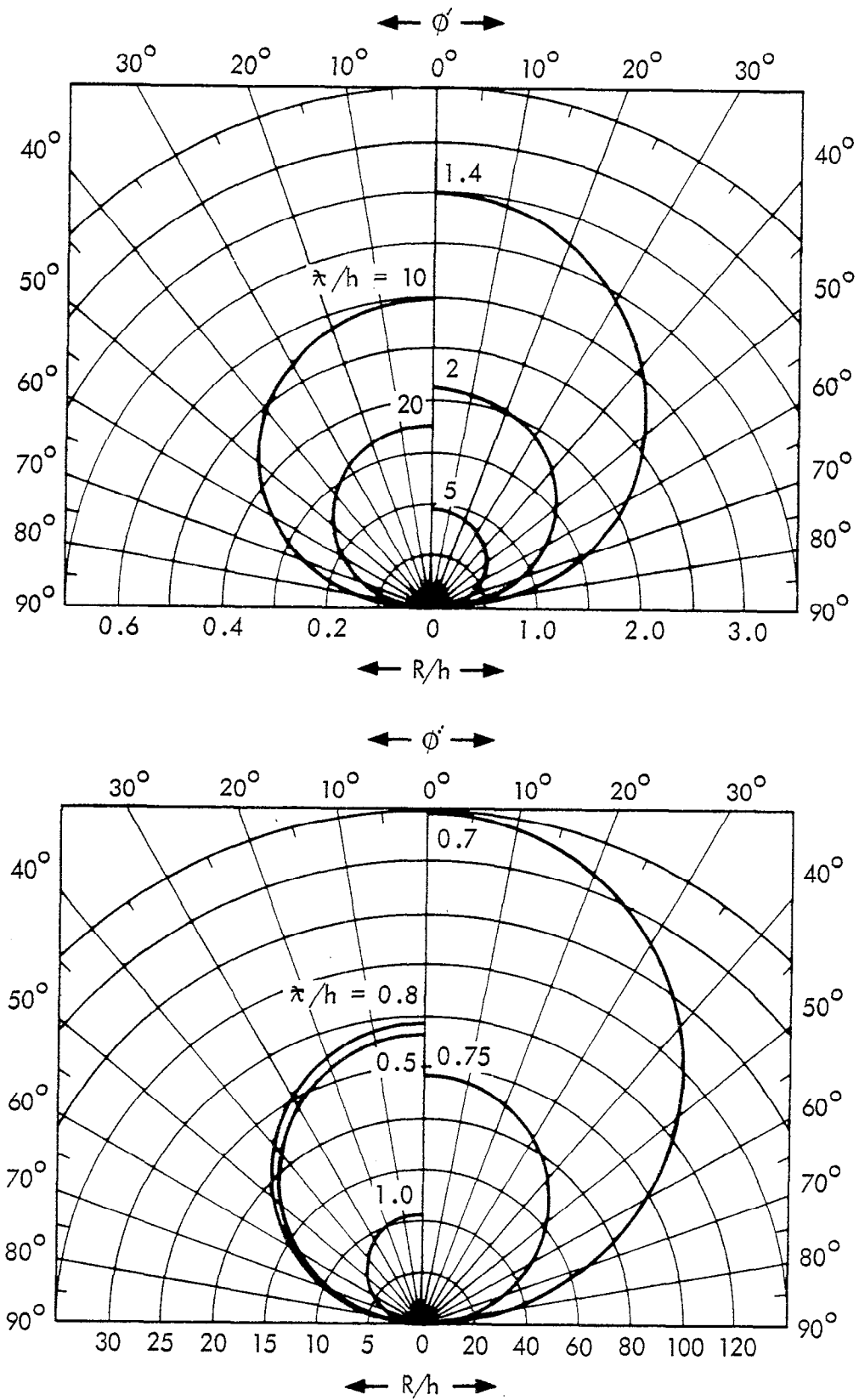


Figure 19. $\frac{\sigma}{\omega \epsilon} \ll 1$, $a/h = 0.001$, $H_0(\lambda/h)\cos\phi/H_0 = 0.01$ vs R/h .

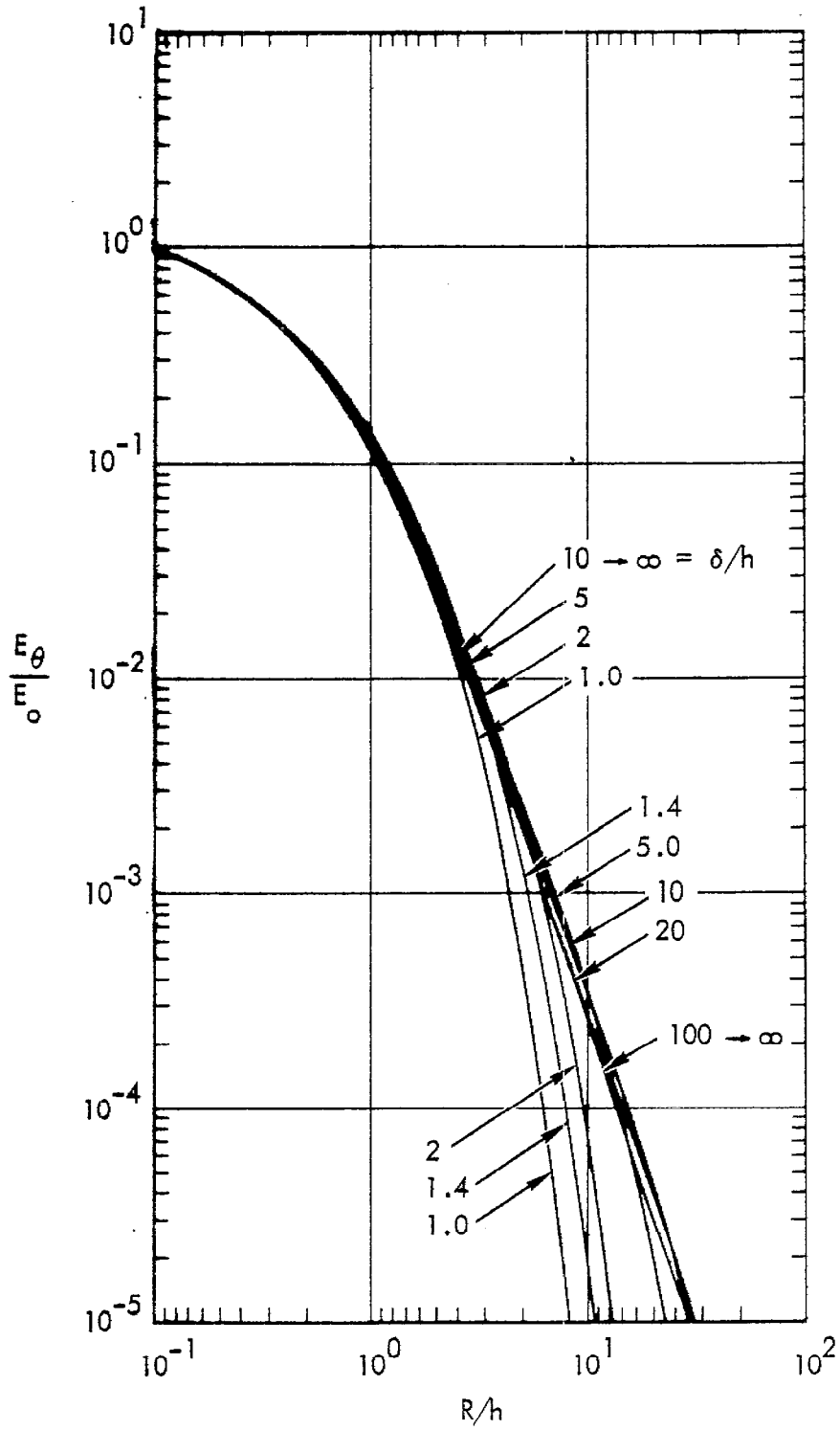


Figure 20. $\frac{\sigma}{w\epsilon} \gg 1$, $a/h = 0.1$, $E_\theta(k/h)/E_0$ vs R/h .

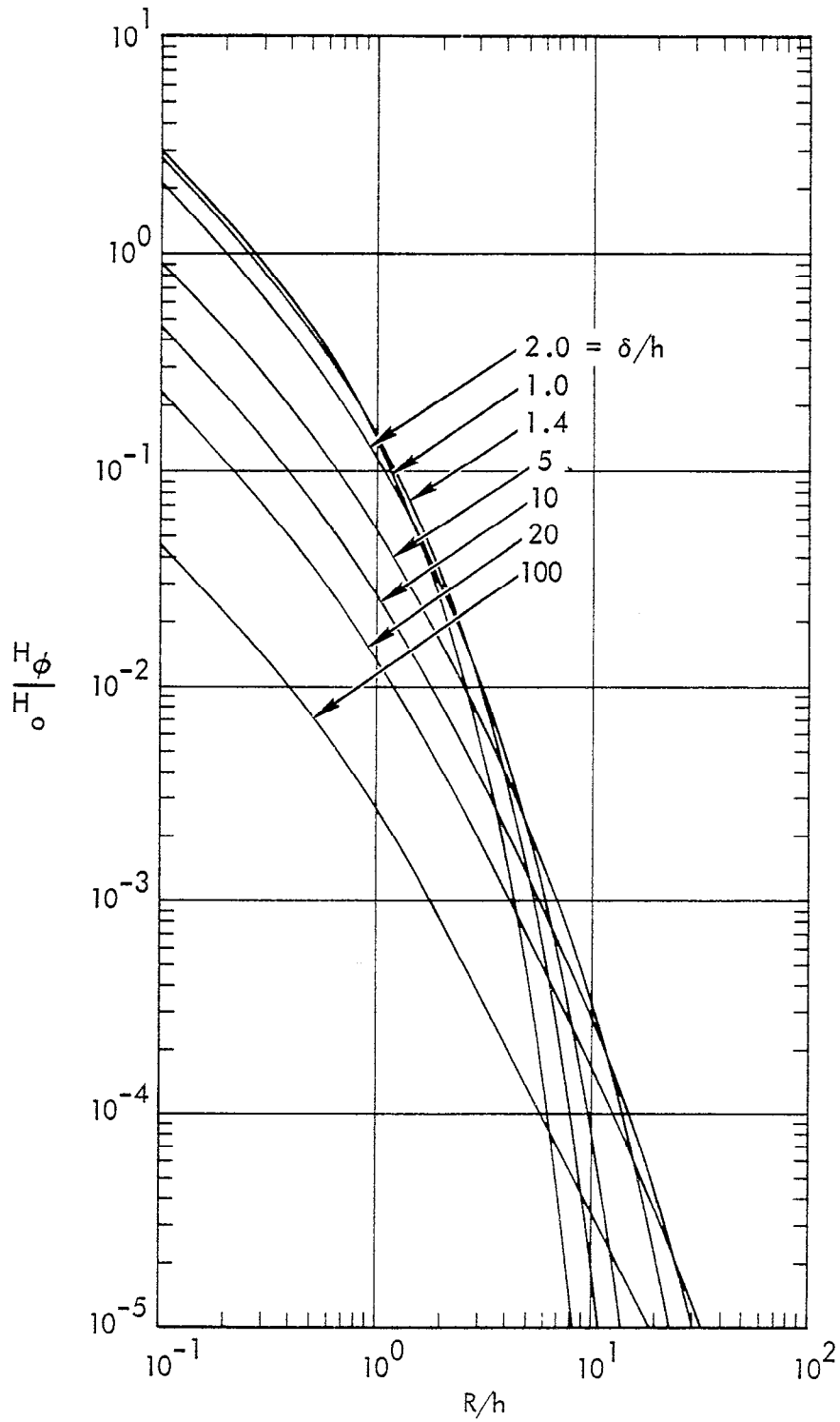


Figure 21. $\frac{\sigma}{w\epsilon} \gg 1$, $a/h = 0.1$, $H_0(k/h)/H_0$ vs: R/h .

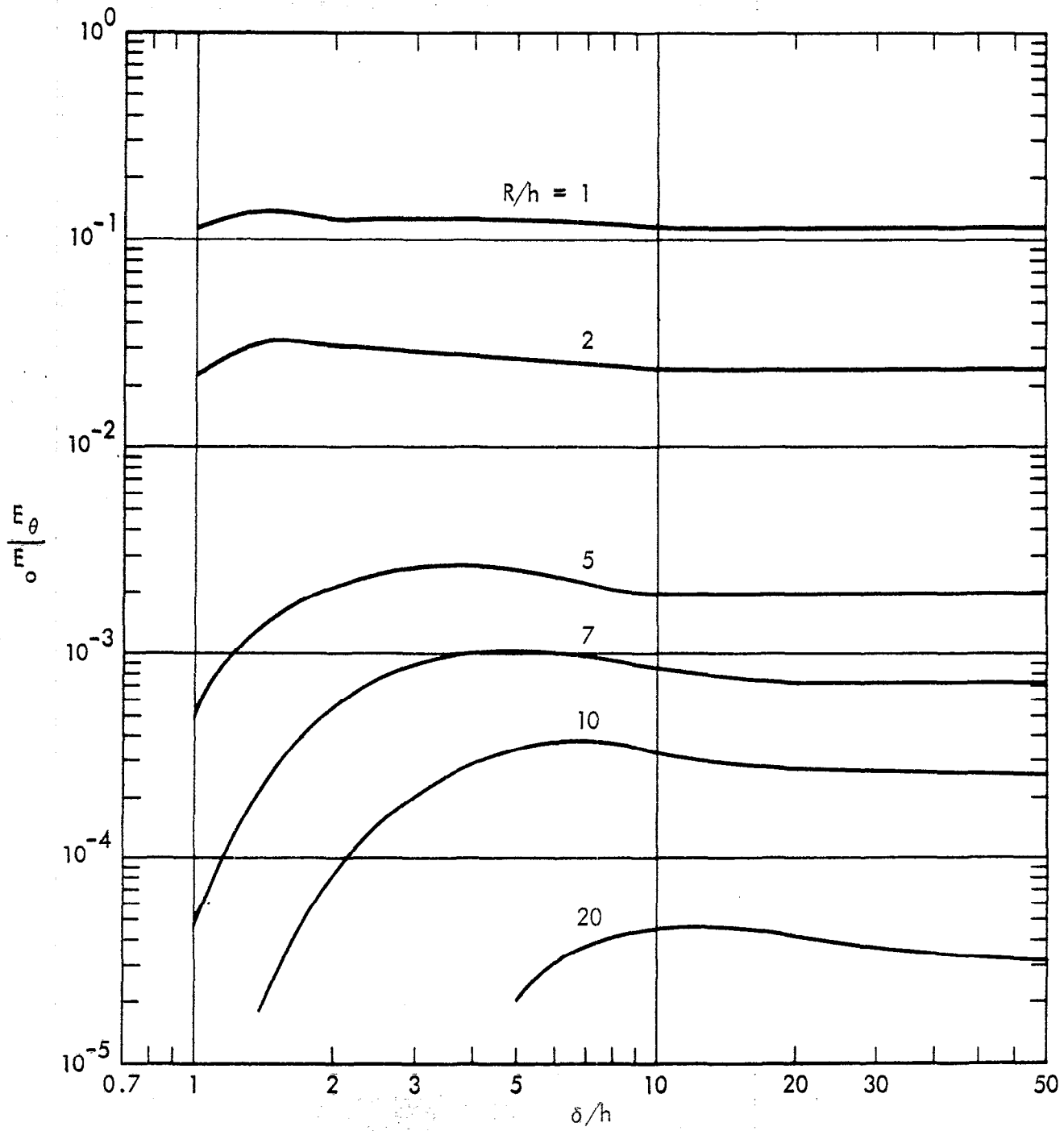


Figure 22. $\frac{\omega a}{w c} \gg 1$, $a/h = 0.1$, $E_\theta(R/h)/E_0$ vs δ/h .

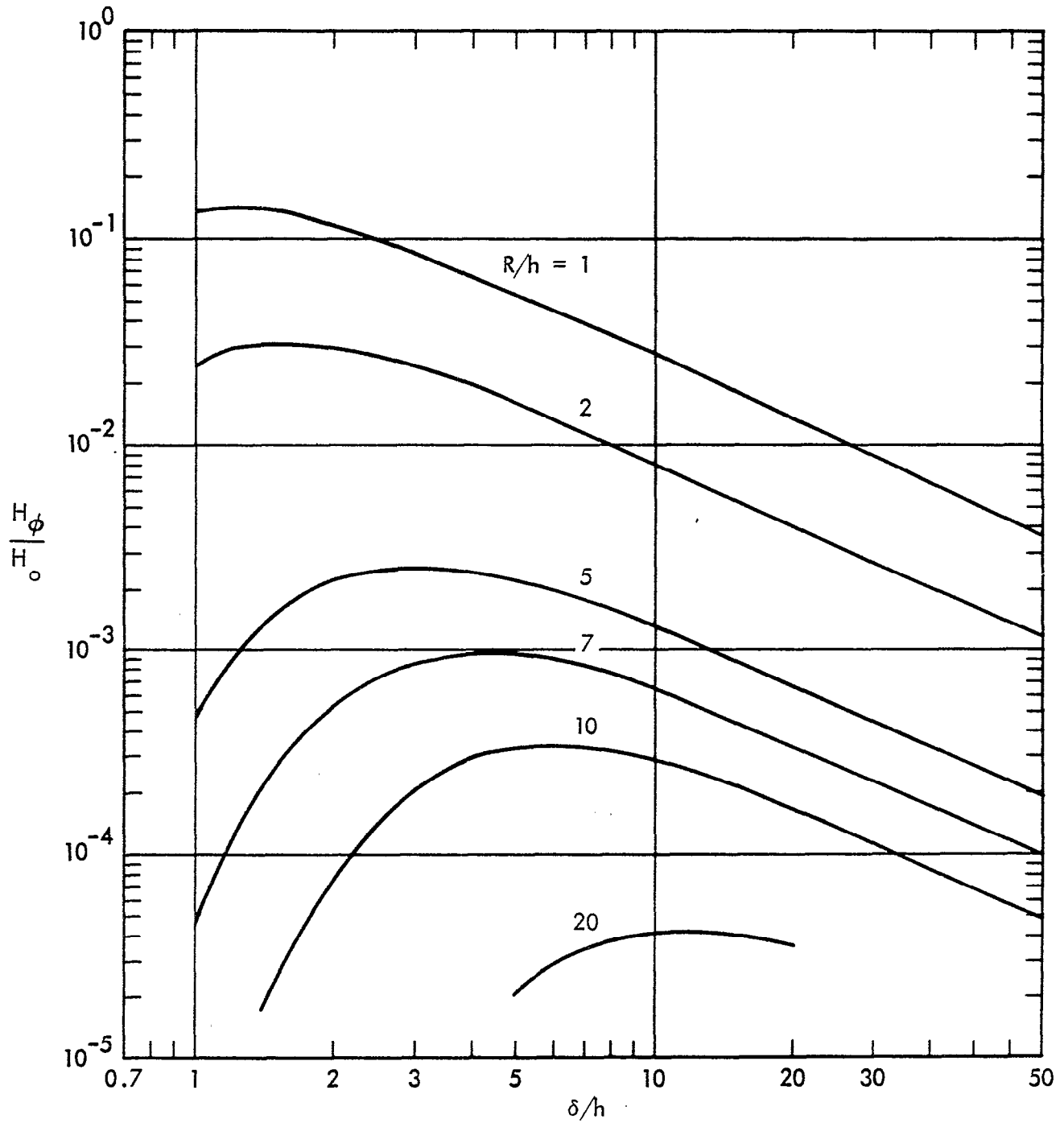


Figure 23. $\frac{\sigma}{\omega \epsilon} \gg 1$, $a/h = 0.1$, $H_0(R/h)/H_0$ vs δ/h .

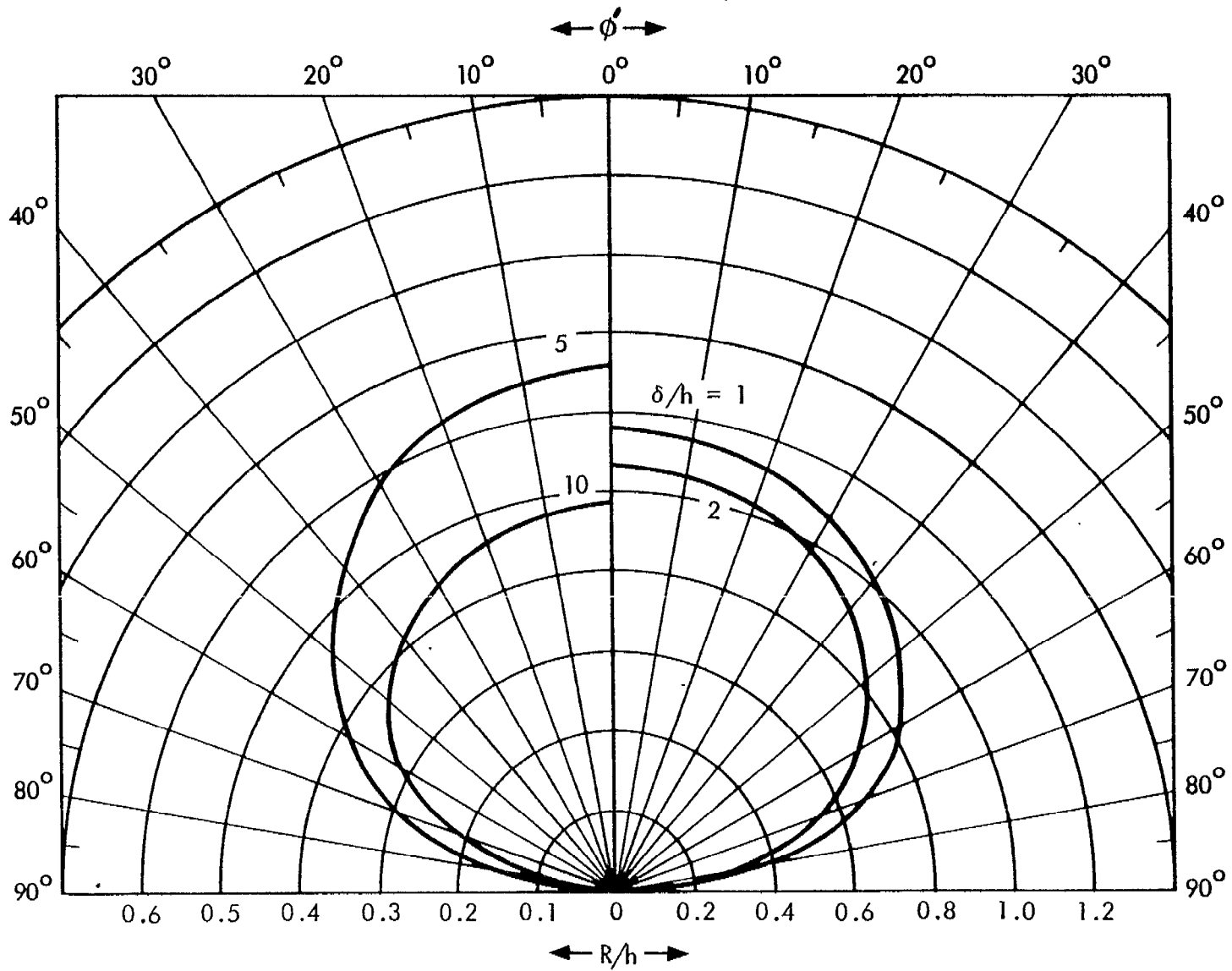


Figure 24. $\frac{\sigma}{w\epsilon} \gg 1$, $a/h = 0.1$, $H_\phi(\kappa/h)\cos\phi'/H_0 = 0.1$ vs R/h .

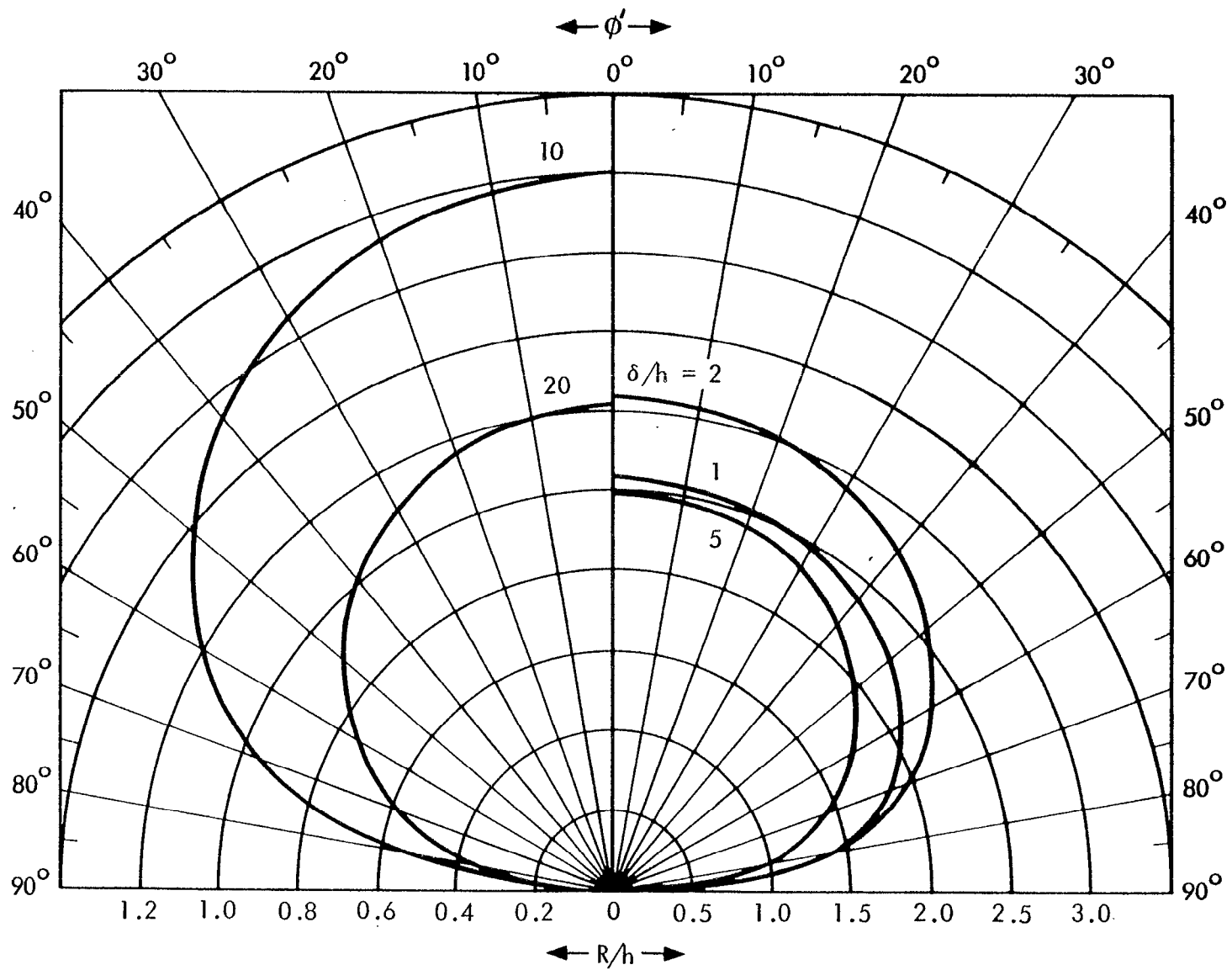


Figure 25. $\frac{\sigma}{\omega \epsilon} \gg 1$, $a/h = 0.1$, $H_{\phi}(\lambda/h) \cos \phi / H_0 = 0.01$ vs R/h .

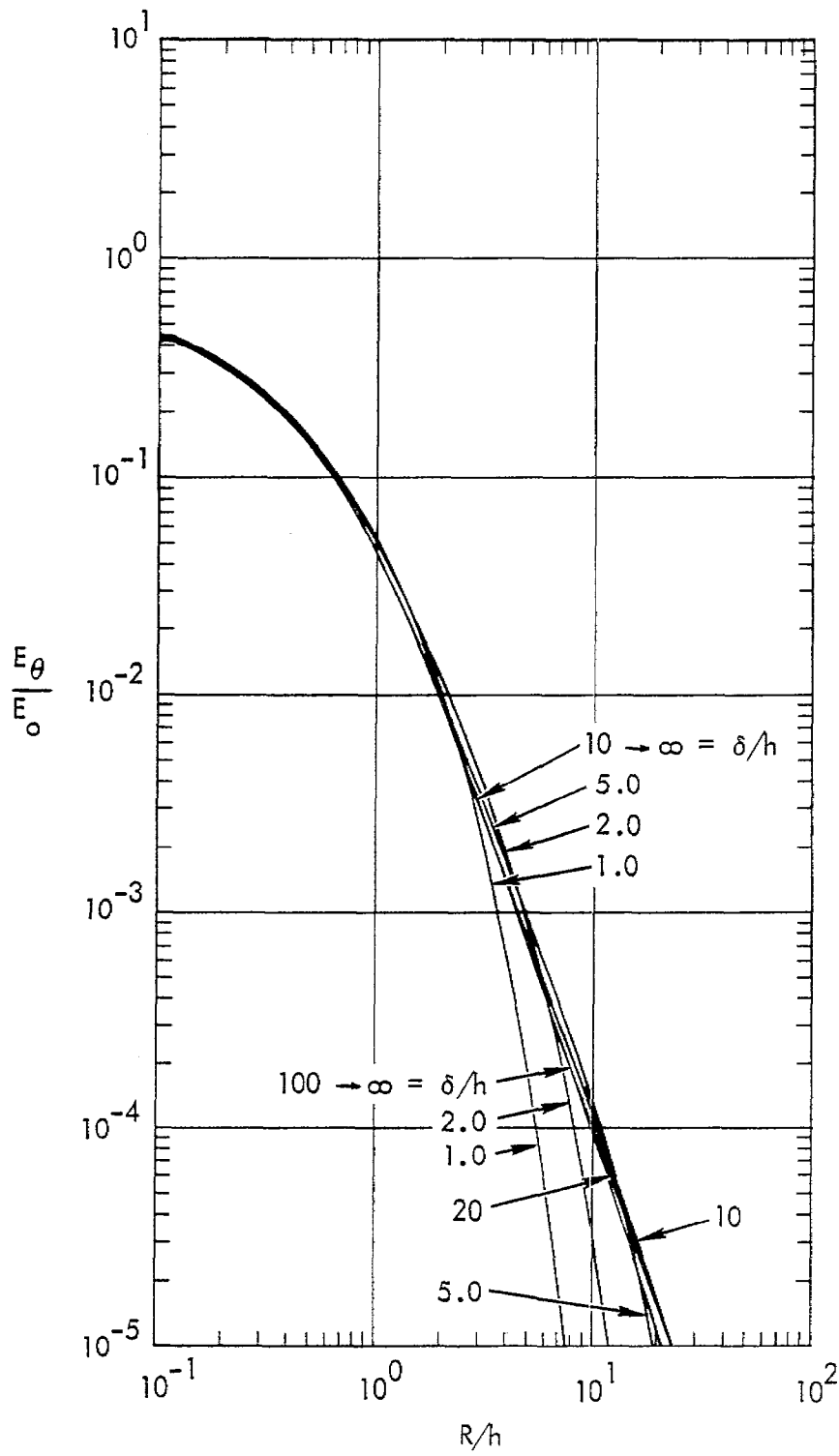


Figure 26. $\frac{\sigma}{\omega\epsilon} \gg 1$, $a/h = 0.01$, $E_\theta(\lambda/n)/E_0$ vs R/h .

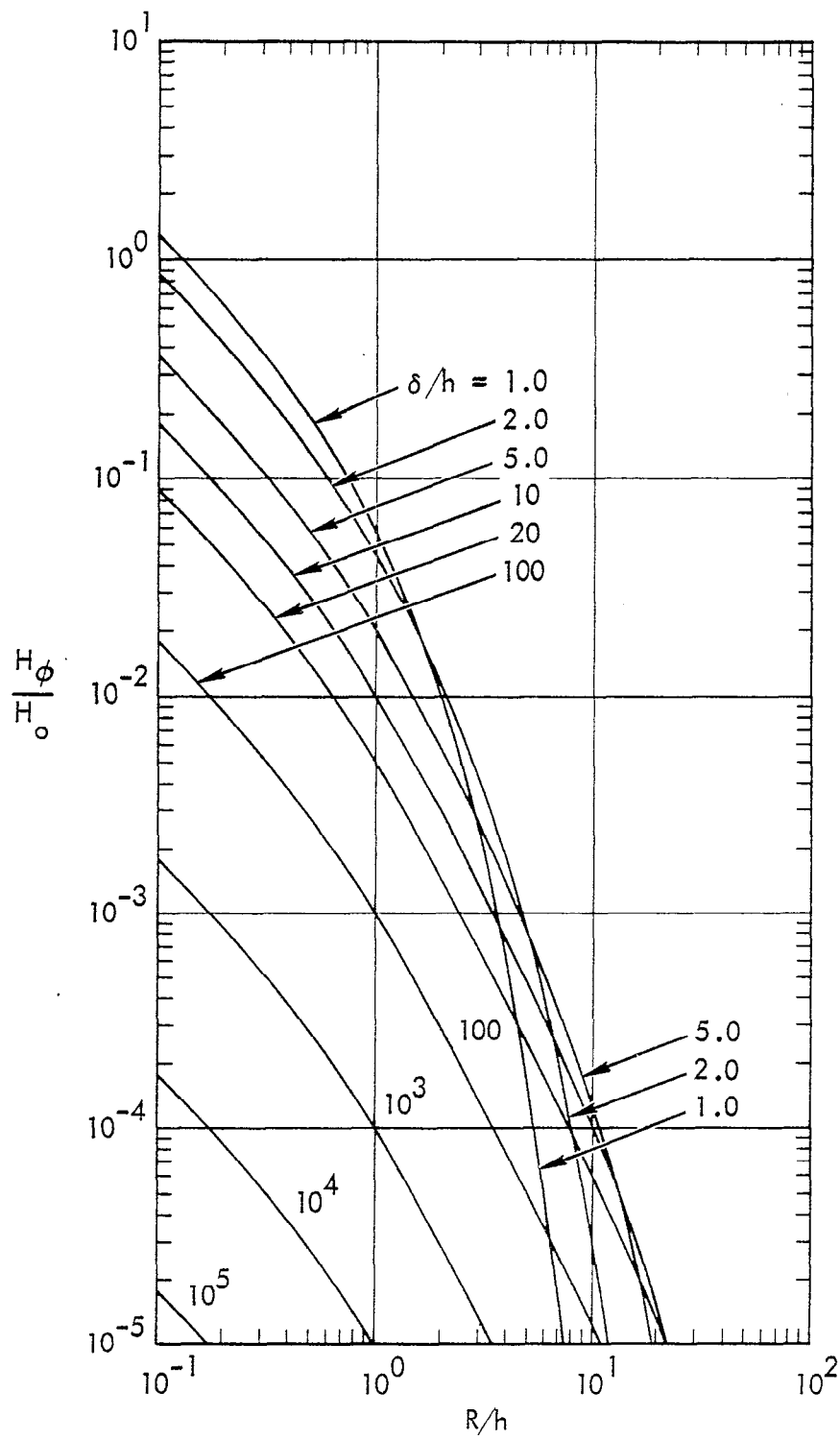


Figure 27. $\frac{\sigma}{w\epsilon} \gg 1$, $a/h = 0.01$, $H_\phi(k/h)/H_0$ vs R/h .

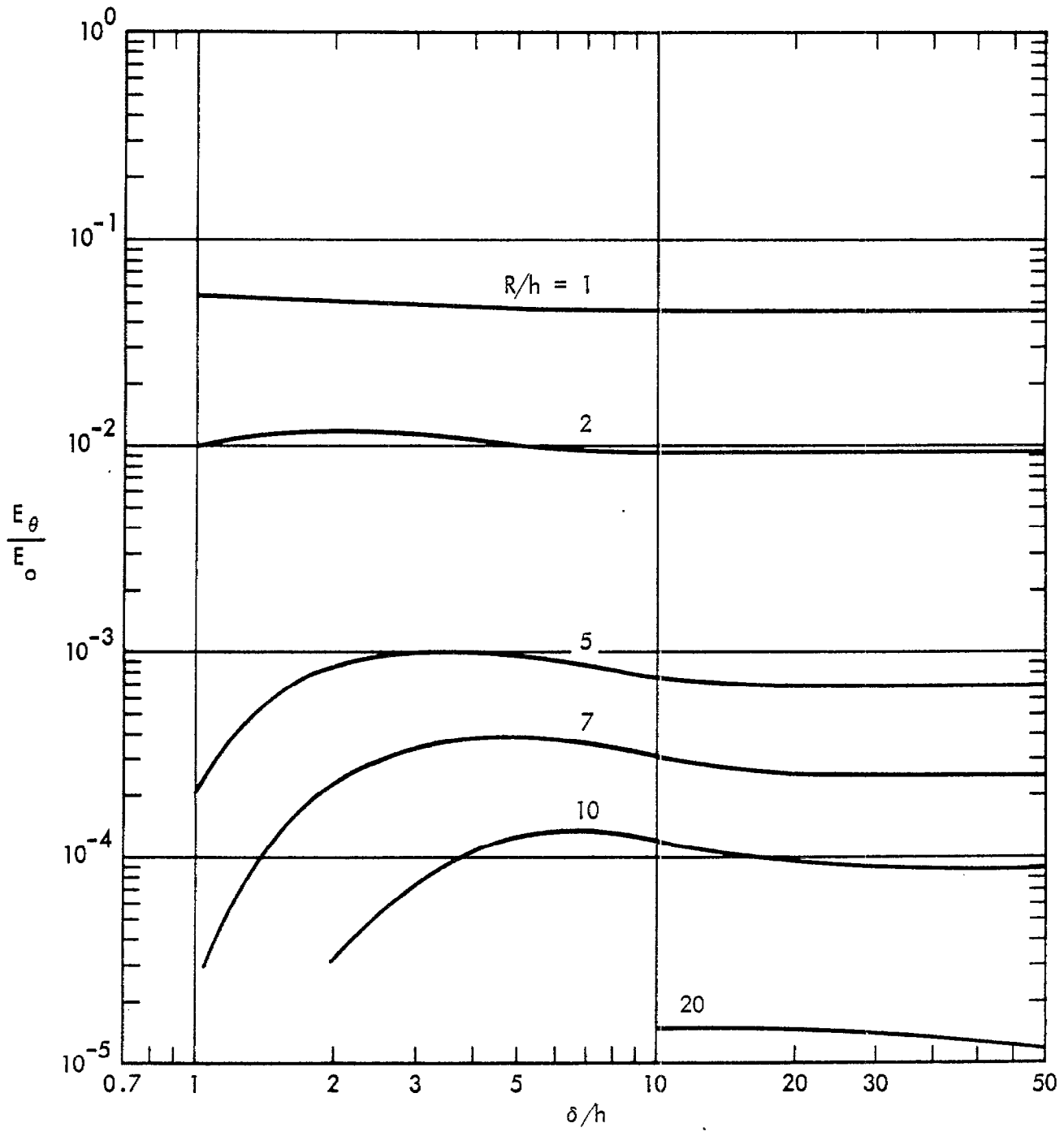


Figure 28. $\frac{\omega^2}{\omega_c^2} \gg 1$, $a/h = 0.01$, $E_\theta(R/h)/E_0$ vs δ/h .

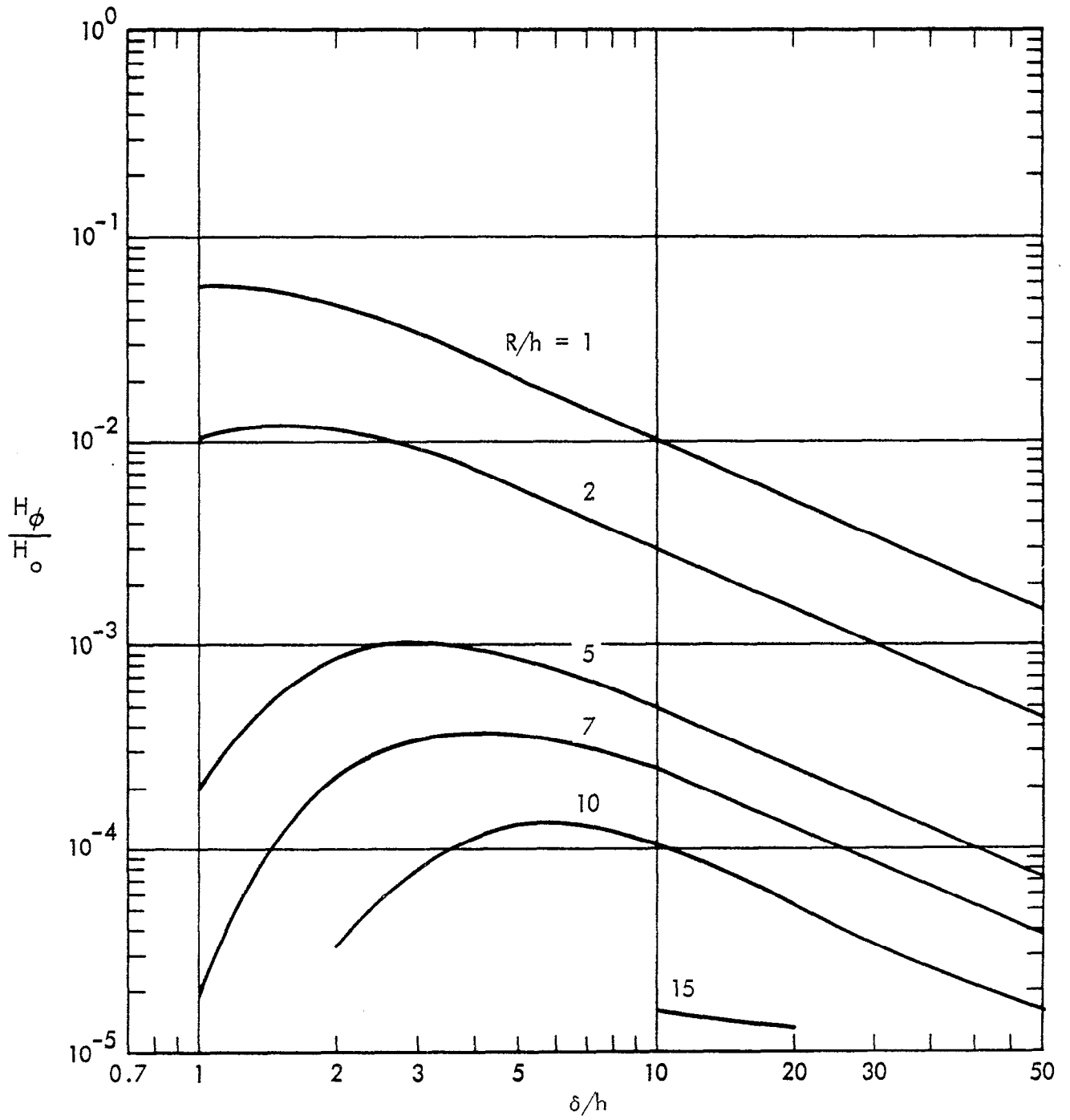


Figure 29. $\frac{\sigma}{\omega \epsilon} \gg 1$, $a/h = 0.01$, $H_\phi(R/h)/H_0$ vs δ/h .

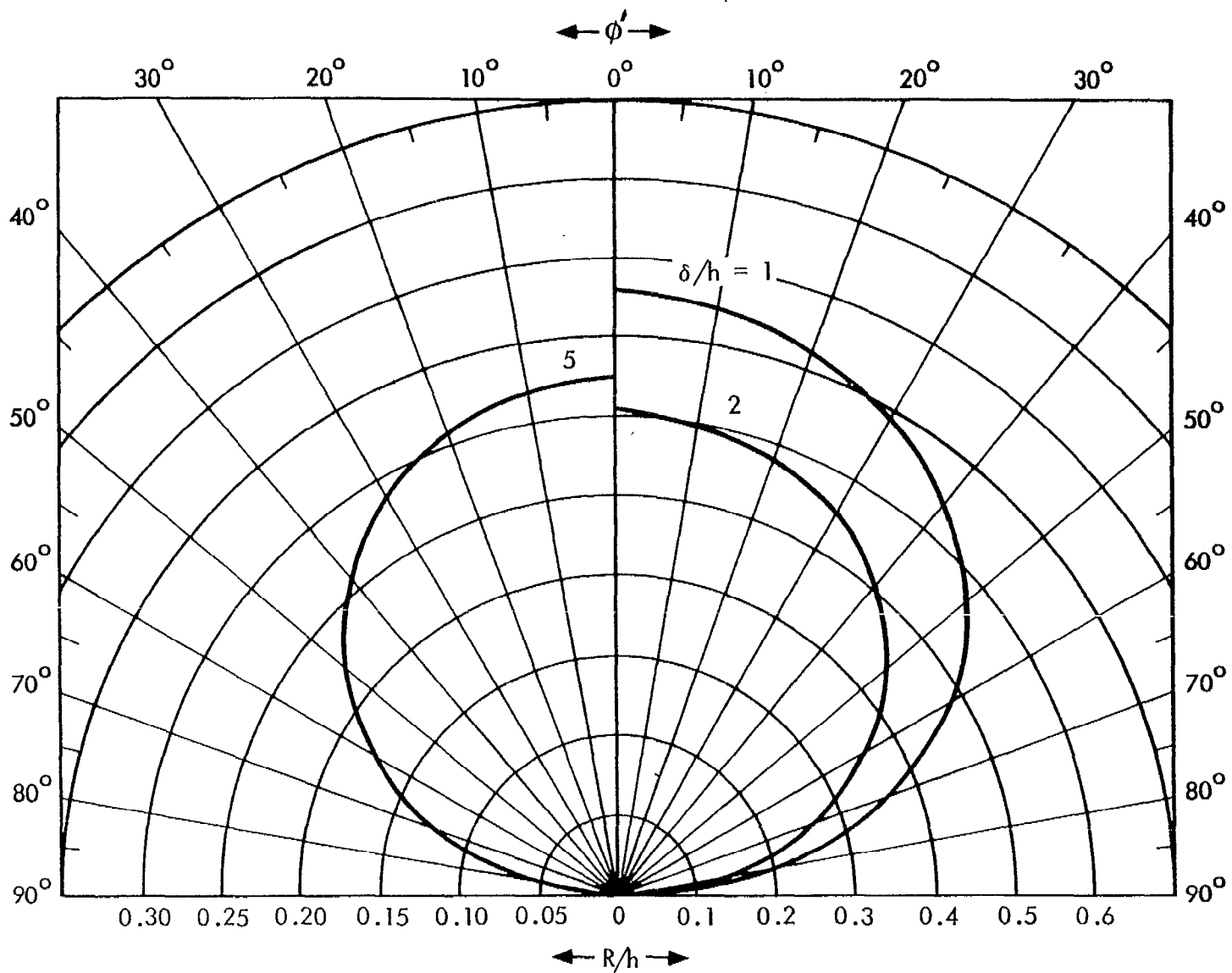


Figure 30. $\frac{\sigma}{\omega \epsilon} \gg 1$, $a/h = 0.01$, $H_\phi(\lambda/h) \cos \phi / H_0 = 0.1$ vs R/h .

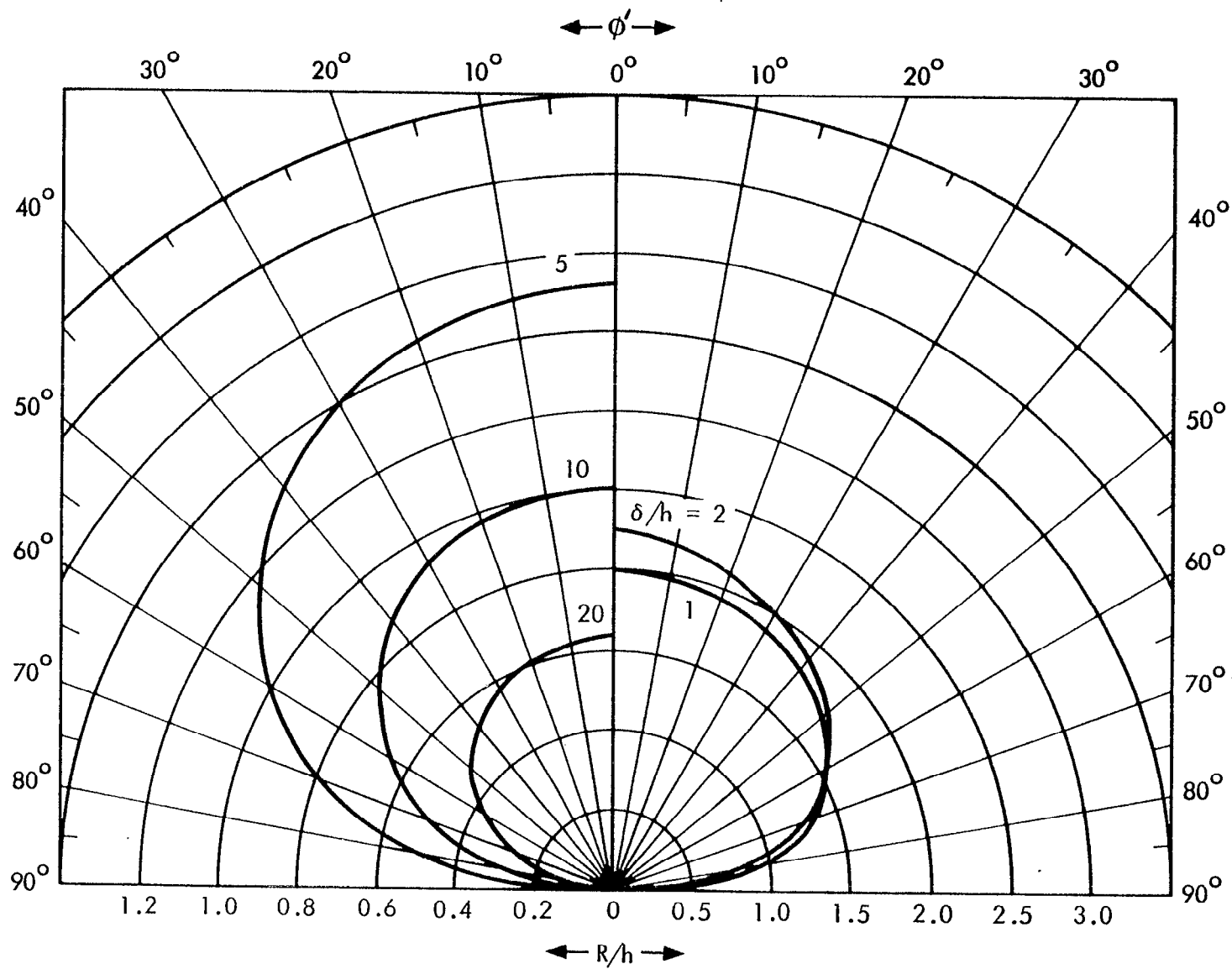


Figure 31. $\frac{\sigma}{\omega \epsilon} \gg 1$, $a/h = 0.01$, $H_\phi(\lambda/h) \cos \phi' / H_0 = 0.01$ vs R/h .

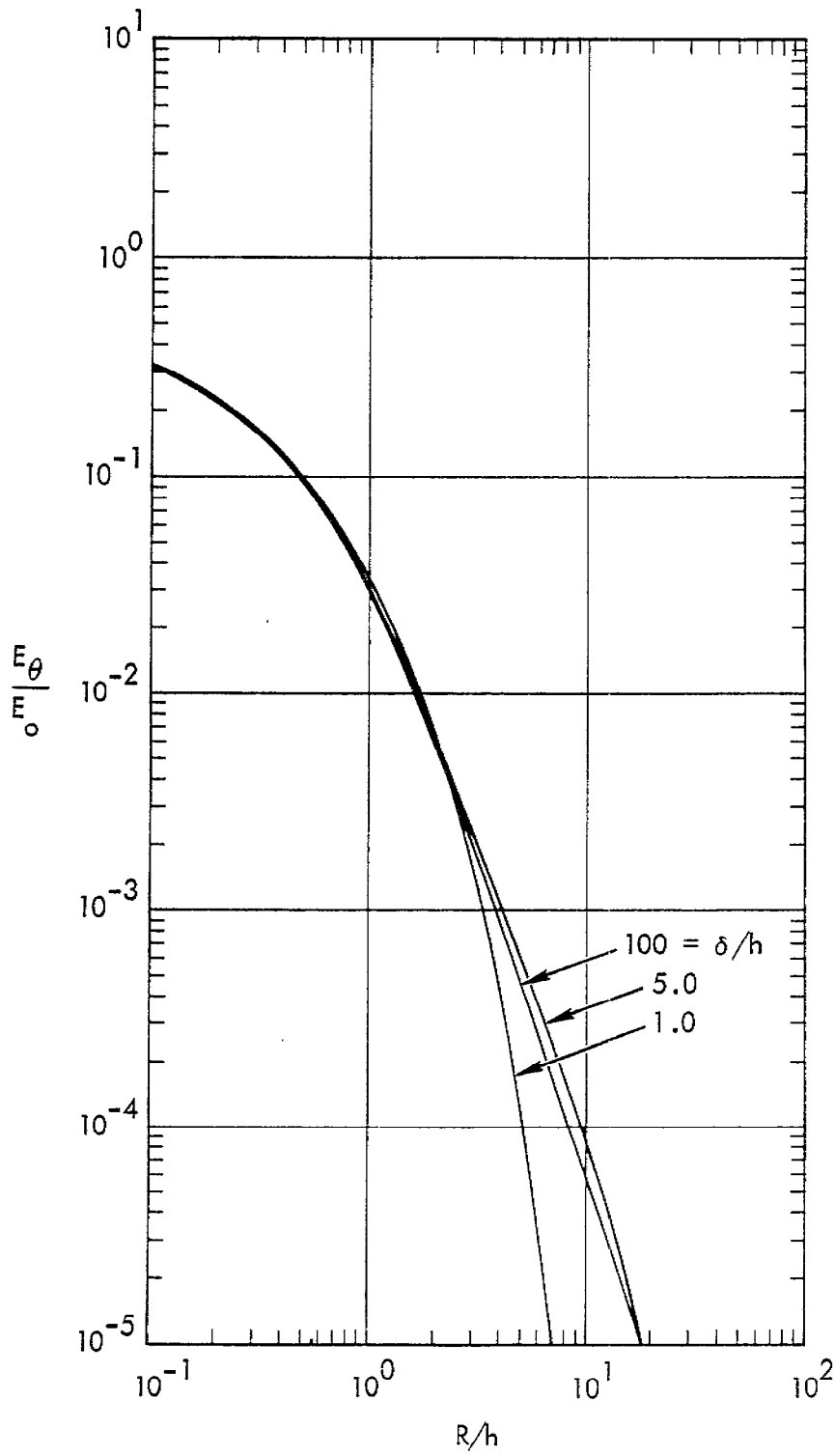


Figure 32. $\frac{\sigma}{\omega\epsilon} \gg 1$, $a/h = 0.001$, $E_\theta(\lambda/h)/E_0$ vs R/h .

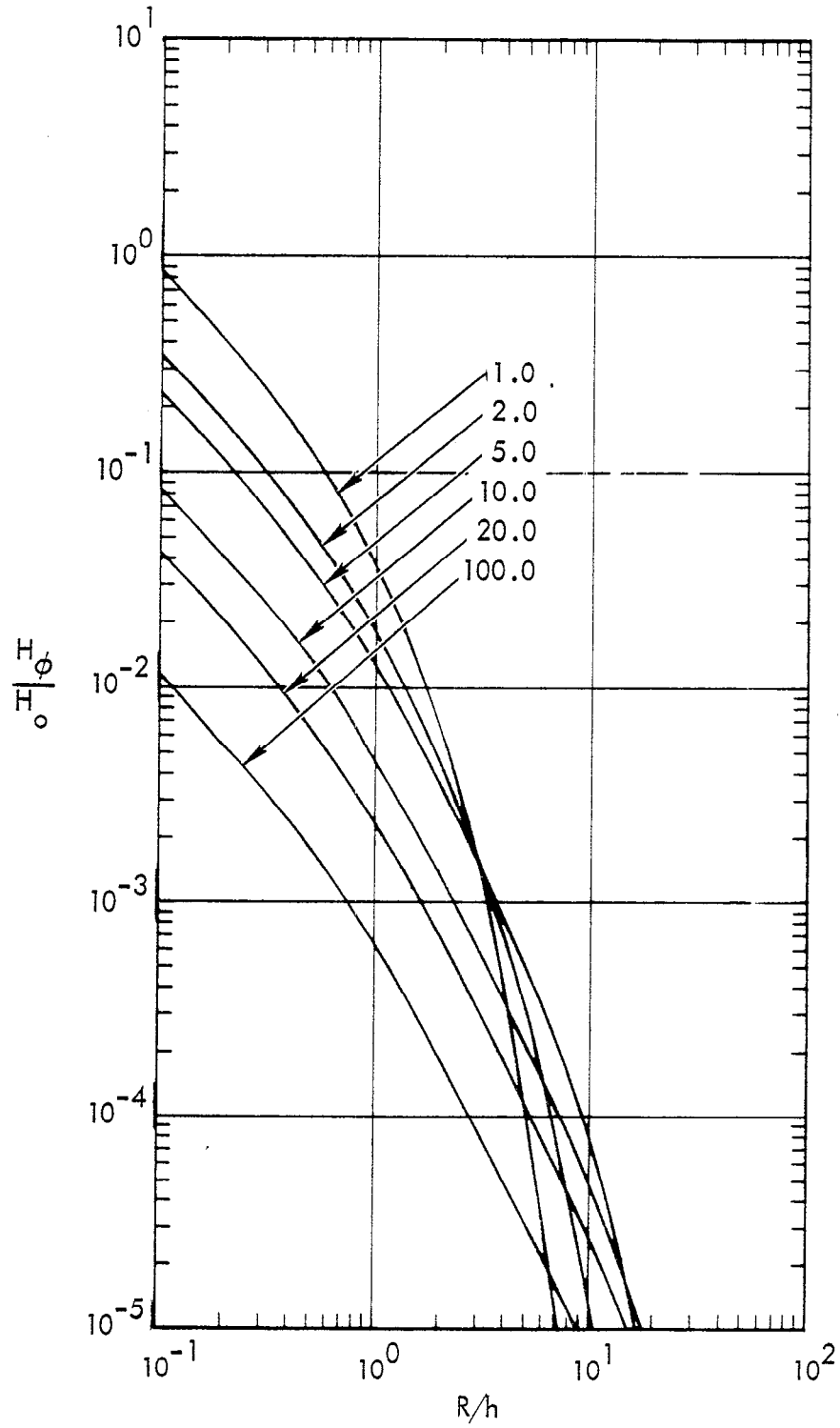


Figure 33. $\frac{\sigma}{\omega \epsilon} \gg 1$, $a/h = 0.001$, $H_0(\lambda/h)/H_0$ vs R/h .

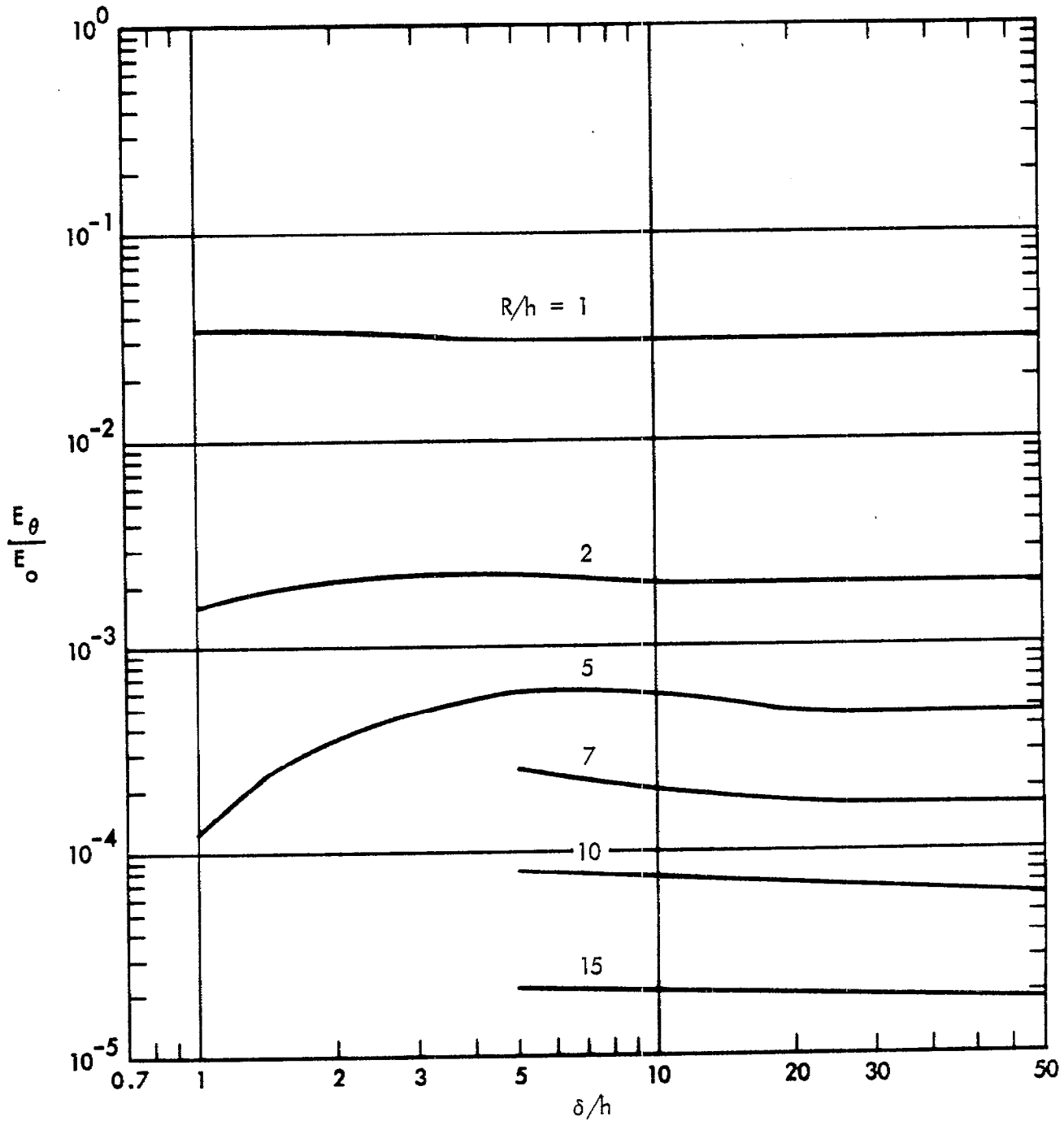


Figure 34. $\frac{\sigma}{w\epsilon} \gg 1$, $a/h = 0.001$, $E_\theta(R/h)/E_0$ vs δ/h .

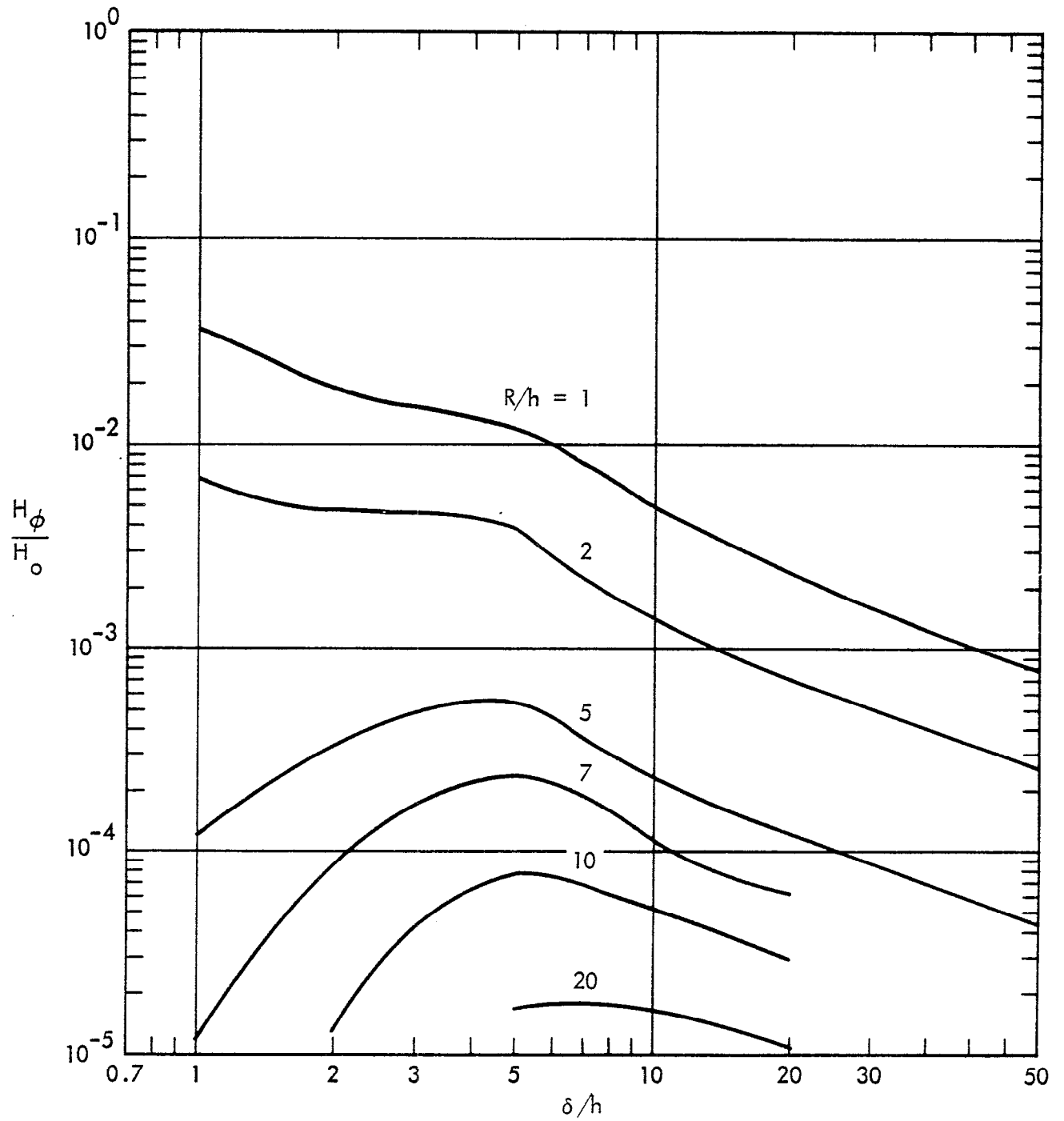


Figure 35. $\frac{\sigma}{w\epsilon} \gg 1$, $a/h = 0.001$, $H_\phi(R/h)/H_0$ vs δ/h .

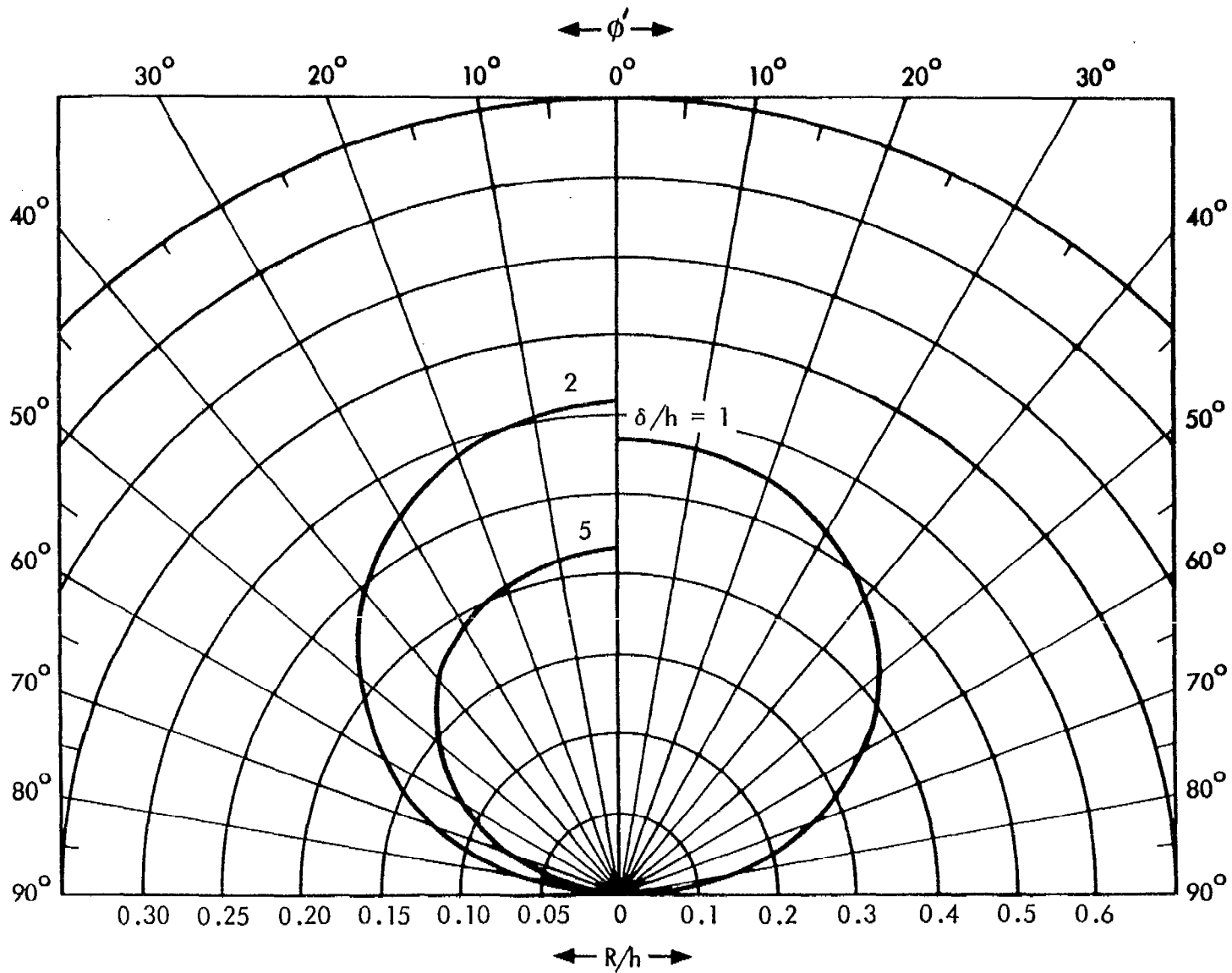


Figure 36. $\frac{\sigma}{w\epsilon} \gg 1$, $a/h = 0.001$, $H_\phi(\lambda/h)\cos\phi'/H_0 = 0.1$ vs R/h .

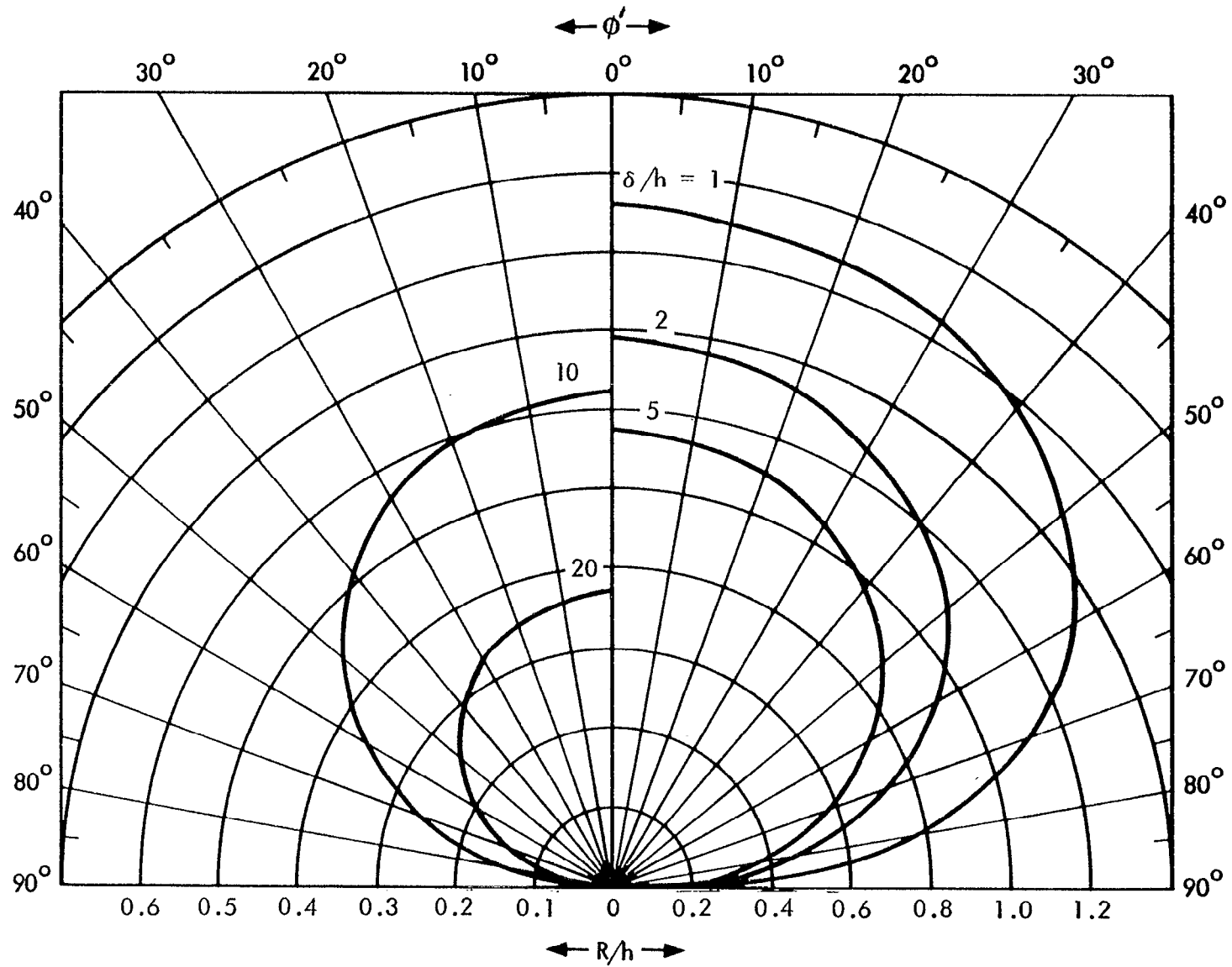


Figure 37. $\frac{\sigma}{w\epsilon} \gg 1$, $a/h = 0.001$, $H_\phi(\lambda/h)\cos\phi'/H_0 = 0.01$ vs R/h .

SECTION 4.0

VERIFICATION AND COMMENTS ON THE RESULTS

4.1 PREDICTED ACCURACY

No general analytical method has been found for relating the accuracy of a field computation to the number of current zones. Reasonable physical and theoretical arguments have been made for choice of $N \geq h/a$, but the value of λ/h no doubt also has an effect. By employing $N = 32$ for $h/a = 10$, and $N = 100$ for $h/a = 100$, errors in the current distributions due to the zoning have been limited to $\pm 2\%$ for $R/h \geq 0.2$. For $h/a = 1000$, $N = 256$ was used, and the results are less accurate than for the other cases. This was a necessary limitation imposed by inefficiency of the FORTRAN-IV version of the matrix inversion routine employed for work on the CDC 6600 machine. Larger values of N could have been used for computation with the CDC 3600 computer, for which a machine-language program had been prepared, but this would have increased costs considerably. Nevertheless, the inaccuracy in the field data for $h/a = 1000$ is believed to be less than several percent because of the empirical finding that relative errors in the fields are much less than the errors in the corresponding current distributions.

4.2 COMPARISON WITH THEORY

4.2.1 The Case $\sigma/(w\epsilon) \ll 1$. A detailed theoretical expression for the scattering cross section of a cylinder is given in King's treatise on antennas⁴ but it has not yet been evaluated for the precise values of h/a used here. Nevertheless a rough check can be made. The backscattering cross section is related to the scattered field by

$$\sigma_b/\lambda^2 = (E/E_0)^2 4\pi R^2/\lambda^2, \quad (11)$$

so that

$$E/E_0 = (\pi)^{\frac{1}{2}} (\kappa/h) (\sigma_b/\lambda^2)^{\frac{1}{2}} (R/h)^{-1} \quad (12)$$

In the reference (page 508), plots of σ_b/λ^2 are given for values of Ω (the Hallén parameter) corresponding nearly to our cases of $h/a = 100$ and 1000 . We compare values at the first resonance, for a distance $R/h = 10$, which is sufficiently great to correspond to the radiation zone. Note that the value of κ/h was obtained from our Figures 10 and 16, as were the E-values for comparison.

First-Order Theory					Machine	
Ω	h/a	κ/h	σ_b/λ^2	E/E_0	h/a	E/E_0
10	75	0.685	1.01	0.122	100	0.112
15	900	0.670	0.92	0.114	1000	0.100

For sufficiently great distances from the post ($R/h \gtrsim 2$) the dependences on R and λ should match those for a short electric dipole.³ Thus both E and H fall off as $(R/h)^{-1}$ for $R/h \gtrsim 5 \lambda/h$. Note that this criterion for radiation-zone behavior depends upon electrical length of the scatterer as well as relative distance. At fixed R/h in this regime the fields decrease as $(\lambda/h)^{-2}$, until λ/h becomes large enough to violate the condition on it. If $2 \lesssim R/h \lesssim \lambda/h$, the near-zone dependences are $(R/h)^{-3}$ for E , and $(R/h)^{-2}$ for H . Here E becomes independent of λ/h , i.e., it is quasi-static, whereas H falls off as $(\lambda/h)^{-1}$, and approaches zero as the charge distribution becomes static.

For $R/h \lesssim 2$, the effects of finite size of the scatterer are important. At the surface of the post, the scattered field is equal and opposite to the incident to meet the boundary condition for large surface conductivity. The scattered magnetic field depends upon surface current and adds to the incident field. It is dependent upon the effective center impedance of the scatterer, which may be easily shown to be about 70 ohms for the dipole, or 35 ohms for the post, for resonance.

The quasi-static electric-field values have been checked against the results of a variational approximation to the field due to a hollow conductive cylinder placed in a

uniform electric field. The method is novel and revealing, although the result is implied in a familiar textbook problem⁵. It is found that the static field is

$$E/E_0 = (R/h)^{-3} [3 \ln(4h/a) - 7]^{-1} .$$

Comparisons are made in the table below:

R/h	h/a	Variational	Machine	100(M-V)/V = % error
10	10	2.46×10^{-4}	2.40×10^{-4}	-2.3
	100	9.09×10^{-5}	9.0×10^{-5}	-1.0
	1000	5.59×10^{-5}	5.8×10^{-5}	+3.6
40	10	3.842×10^{-6}	3.810×10^{-6}	-0.83
	100	1.423×10^{-6}	1.415×10^{-6}	-0.56
	1000	8.737×10^{-7}	8.366×10^{-7}	-4.25

The agreement is satisfactory, although there is again reason to believe that the number of zones was too small in the computations for $h/a = 1000$.

Further checks can be made at the optical limit, $\lambda/h \ll a/h$, when the computations are extended to wavelengths shorter than for the first resonance.

4.2.2 The Case $\sigma/w\epsilon \gg 1$. The effect of a conducting medium surrounding the post is to attenuate the scattered wave rapidly, with the attenuation rate greatest for the smaller values of δ/h . For $\delta/h \gtrsim 5$ for the electric field or $\delta/h \gtrsim 20$

for the magnetic field the field ratios are approximately the same as those for the same values of κ/h in the quasi-static limit of the non-conducting case. This is not particularly surprising, because the propagation constant ($2\pi/\lambda$) is essentially equal to the skin depth (δ) for plane-wave propagation in a conducting medium. The details have not been investigated due to the limited usefulness of these data. The positions of the rather broad resonances do not occur within a narrow range of λ/h values, independent of R/h , as for the non-conducting case. In fact the value of δ/h for which resonance occurs shifts to higher values about as R/h , with $2\delta/h \approx R/h$ at the peak, for the range of values plotted.

4.3 COMPARISON WITH EXPERIMENT

Sevick has measured the backscattering cross sections of silver-plated steel rods having $a = 3.5 \times 10^{-2}$ cm at a fixed wavelength of $\lambda = 10.0$ cm⁶. He varied κ/h by varying the length h , so a/h was not constant. Therefore, comparison with our data provides only a rough check, but the agreement is encouraging, as shown in Figure 38. Equation 12 was used for converting values of σ_E/λ^2 to equivalent field ratios, E/E_0 .

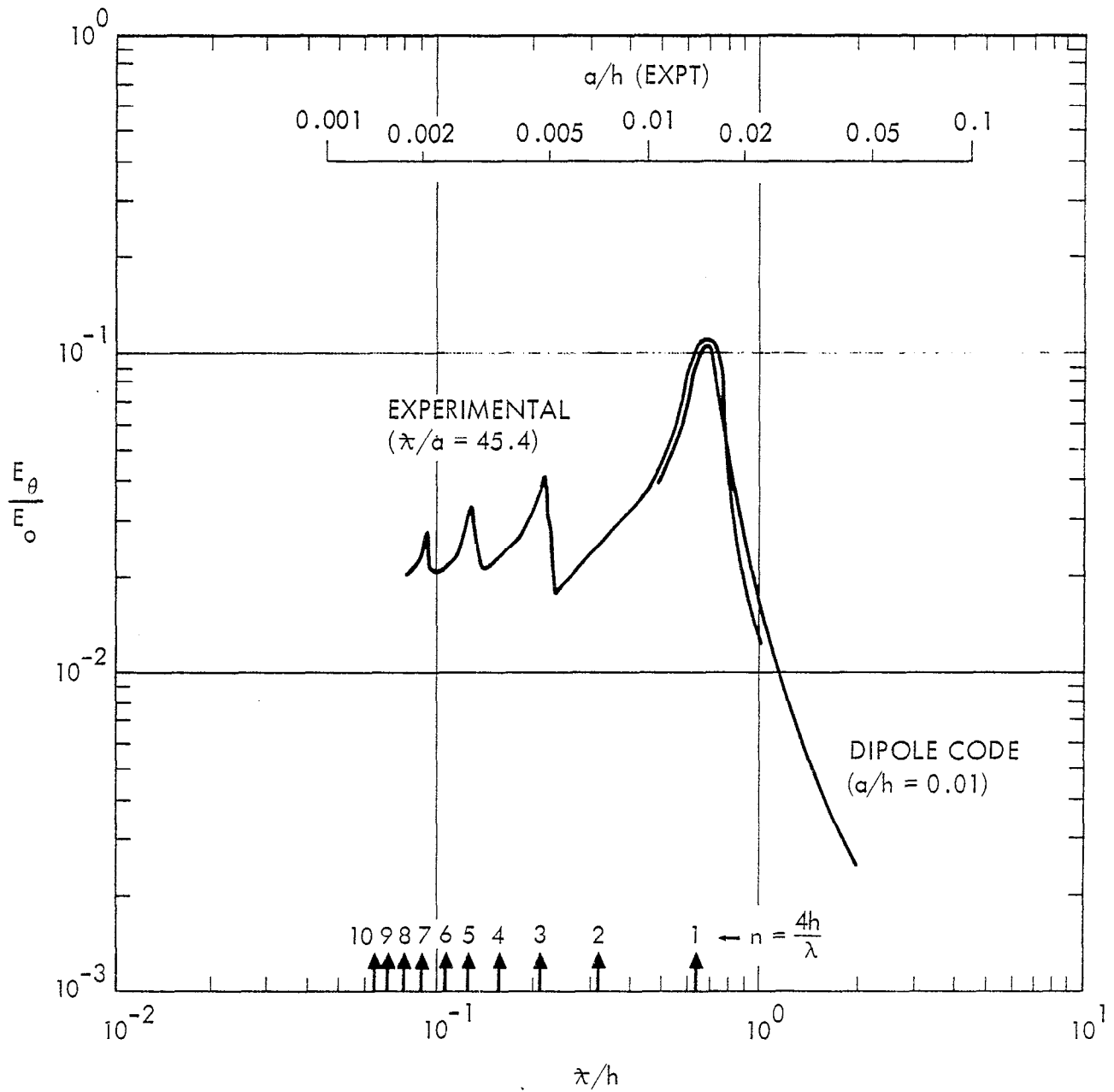


Figure 38. A comparison with experiment for the first resonance of E_θ/E_0 ($\frac{\sigma}{\omega\epsilon} \ll 1$, $R/h = 1$).

SECTION 5.0
COMPUTER PROGRAMS

Antenna currents were computed with DIPOLE, and electric and magnetic fields with FIELD. A practical necessity for use of DIPOLE is an efficient matrix inversion routine. We have used MLRT^{*}, which, in the COMPASS version for the CDC 3600 machine will invert well-conditioned matrices up to 1000 x 1000 in size. The ASCENT version has not been written, so a FORTRAN-IV version was used for computations on the CDC 6600 machine, with a resultant limitation to matrices smaller than about 256 x 256. About 90 seconds of central-processor time were required for a typical $N = 256$ problem on the CDC 6600, and this time varies approximately as N^3 . Additional peripheral-processor time is, of course, required. Although not discussed above, the current distributions are also available, as are the phase angles for the FIELD output. Arbitrary scattering angles may be assumed.

Related programs have also been written although they are not yet operational: FOREST will solve the scattering problem for an array of perfectly conducting dipoles of various lengths, all dipoles assumed normal to the same symmetry plane. This is equivalent to an array of dipoles normal to a common perfectly conducting plane. MAZE will solve the scattering problem for an array of perfectly conducting dipoles of various lengths, with the dipoles at random positions and orientations.

* MLRT is a Northrop Corporation proprietary program. All the other named programs were developed with Air Force funds.

With the availability of an efficient FOURIER inversion program, transient scattering problems may be solved for a wide variety of practical geometries. Loaded scatters, as well as geometries more complex than the cylinder can be dealt with by these techniques although the practical difficulties are generally formidable. In fact other investigators have successfully solved specialized problems involving rotational symmetry.

REFERENCES

1. "Electromagnetic Scattering and Radiation by the Integral Representation Method: I. Arbitrary Configurations of Perfect Conductors," John G. Trulio and J. Randall Coleman, Northrop Ventura Report NVR 2798 (1 August 1963).
2. Theory of Electromagnetic Wave Propagation, Charles Herach Papas (McGraw-Hill, 1965).
3. Electromagnetic Theory, Julius Adams Stratton (McGraw-Hill, 1941).
4. The Theory of Linear Antennas, Ronald W.P. King (Harvard Univ. Press, 1956). (See page 508.)
5. Electrodynamics of Continuous Media, L.D. Landau and E.M. Lifshitz (Pergamon and Addison-Wesley, 1960). (See page 19.)
6. The Scattering and Diffraction of Waves, Ronald W.P. King and Tai Tsun Wu (Harvard Univ. Press, 1959). (See page 103 and 153.)